Sensor Development for Liquid Water Detection in Dry Storage Casks: FY19 Status

Spent Fuel and Waste Disposition

Prepared for
US Department of Energy
Spent Fuel and Waste Science and Technology

Pacific Northwest National Laboratory
Ryan M. Meyer, Morris S. Good, Jonathan D. Suter, Francesco Luzi, Bill Glass, and Chris Hutchinson

September 16, 2019
SFWD-SFWST-M3SF-19PN010201034
PNNL-29112

SUMMARY

Work was performed in fiscal year 2019 (FY19) to assess the feasibility of detecting water inside of dry storage canisters for used nuclear fuel using sensors that would be mounted on the exterior of the dry storage canister and would not require physical penetration of the confinement boundary. The environment inside of a dry cask storage system (DCSS) confinement is inert and free of water to prevent potential corrosion of used fuel cladding or other internal hardware. However, there is some uncertainty about the amount of residual water potentially left behind in a DCSS after drying processes as operational issues during industrial drying processes could result in incomplete drying. Considering the complex spatial and time-dependent temperature profiles in dry storage casks, water may be in liquid or gas phase depending on location in the cask and how long the cask has been in storage. Direct gas sampling is difficult as it poses a risk to inadvertent radiological releases. The measurement techniques described here can facilitate the direct observation of residual water in the field without risk of radiological material release and help establish operational data that can inform operating and licensing decisions for extended periods of storage.

The FY19 work focused on a typical bare fuel cask because of the use of a bare fuel cask for the collaborative U.S. Department of Energy (DOE) and Electric Power Research Institute (EPRI) demonstration for storage of high burn-up fuel. This cask is an all metal cask with vertical orientation. This report describes the technique explored for water sensing based on the transducer configuration depicted in Figure S-1. The specific technique is based on the generation of guided ultrasonic plate waves that propagate from the transmitter and through the wall of the confinement barrier to the bottom of the cask. The fundamental anti-symmetric plate wave mode, A0, is the primary sensing mode selected for this effort.

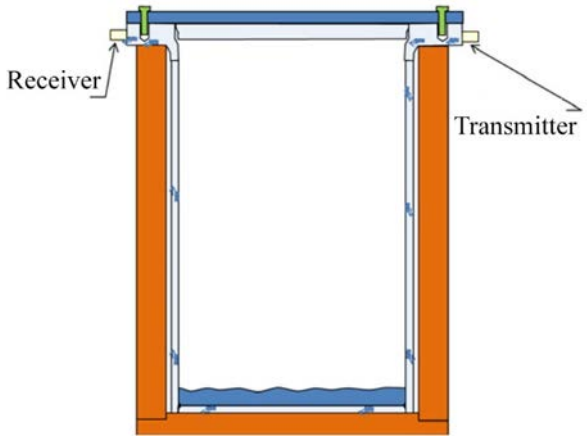

Figure S-1. Depiction of Bare Fuel Cask Showing Target Location of Transmit and Receive Transducer on Canister Lip for Water Detection within Canister

This report documents the laboratory testing performed in FY19 including a description of a mockup to facilitate testing and the test instrumentation with ultrasonic sensors. Several scoping tests were performed in FY19 and are described including the results. These scoping tests included tests to confirm that the A0 mode could be generated in the wall and floor components of the mockup with little interference from the S0 mode, tests to verify that the sound intensity in the mockup could be visualized by utilizing a laser vibrometer, and testing to systematically explore how coupling of the A0 mode through the flange shoulder of the mockup into the side wall of the mockup is impacted by the angle of the transmitter mounted on the flange surface.

Plans for future work include (1) exploring how coupling of the A0 mode through the flange shoulder of the mockup into the floor of the mockup is impacted by the angle of the transmitter mounted on the

flange surface, (2) exploring how sound field focusing is influenced by array configurations (i.e., number and spacing of transducers), (3) evaluating the sensitivity of the A0 mode to quantities of liquid water on the floor of the mockup, and (4) identifying an opportunity to test a prototype on an actual full-scale system.

ACKNOWLEDGEMENTS

The authors would like to thank Ms. Kay Hass for formatting and editing this document.

This page is intentionally left blank.

CONTENTS

LIST OF FIGURES

LIST OF TABLES

ACRONYMS

DCSS	dry cask storage system
DOE	US Department of Energy
EPRI	Electric Power Research Institute
FY	fiscal year
GUW	guided ultrasonic waves
LDV	laser Doppler vibrometry
PNNL	Pacific Northwest National Laboratory
V_g	group velocity
V_p	variation of phase

This page is intentionally left blank.

SENSOR DEVELOPMENT FOR LIQUID WATER DETECTION IN DRY STORAGE CASKS: FY19 STATUS

1. INTRODUCTION

Work was performed in fiscal year 2019 (FY19) to assess the feasibility of detecting water inside of dry cask storage system (DCSS) for used nuclear fuel using sensors that would be mounted on the exterior of the DCSS and would not require physical penetration of the confinement boundary. The environment inside of a DCSS confinement is inert and free of water to prevent potential corrosion of used fuel cladding or other internal hardware. However, there is some uncertainty about the amount of residual water potentially left behind in a DCSS after drying processes. Considering the complex spatial and time-dependent temperature profiles in dry storage casks, water may be in liquid or gas phase depending on location in the cask and how long the cask has been in storage. A review of drying specifications by several vendors concluded that if the specifications are followed correctly, the residual moisture left behind in DCSSs should present an insignificant risk to cladding degradation (Knoll and Gilbert 1987). A more recent analysis has concluded that much larger quantities of residual water could remain in DCSSs, but the amount would still not be expected to lead to significant corrosion of fuel cladding or other internal components (Jung et al. 2013). Industry drying procedures are mostly prescriptive in nature and operational issues during the process could result in incomplete drying. A summary of operational issues and potential negative impacts of residual water is included in Salazar et al. (2019). Direct gas sampling is difficult as it poses a risk to inadvertent radiological material releases. The measurement techniques described here can facilitate the direct observation of residual water in the field without risk of radiological material release and help establish operational data that can inform operating and licensing decisions for extended periods of storage.

The FY19 work focused on a typical bare fuel cask because of the use of a bare fuel cask for the collaborative U.S. Department of Energy (DOE) and Electric Power Research Institute (EPRI) demonstration for storage of high burn-up fuel. This cask is an all metal cask with vertical orientation. The cask consists of an inner confinement vessel where the fuel basket and fuel reside. This confinement vessel is located inside of a thick carbon steel container that provides physical protection and radiation shielding. The interface between the inner shell and the protective container presents an air-gap that is prohibitive to the propagation of ultrasound. However, the canister has a lip near the top of the cask that is accessible for direct placement of a sensor (Figure 1-1).

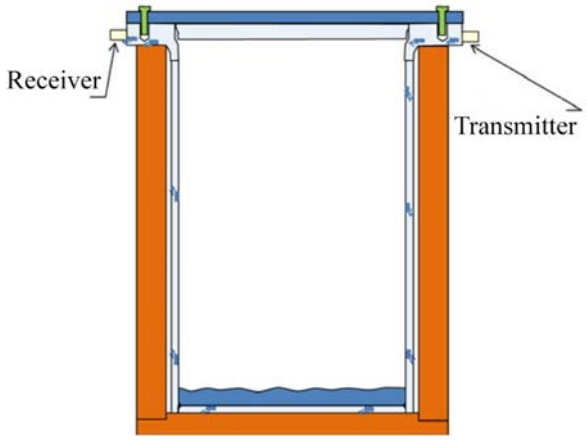

Figure 1-1. Depiction of Bare Fuel Cask Showing Target Location of Transmit and Receive Transducer on Canister Lip for Water Detection within Canister

This report describes the technique explored for water sensing based on the transducer configuration depicted in Figure 1-1. The specific technique is based on the generation of guided ultrasonic waves that propagate from the transmitter and through the wall of the confinement barrier to the bottom of the cask. The fundamental anti-symmetric Lamb wave mode, A0, is the primary sensing mode that is targeted for this application. The overall approach to developing the sensor technology is experimental and is focused on optimizing the A0 mode energy that gets coupled into the wall and floor components of the mockup and then exploring the sensitivity to quantities of liquid water.

A brief introduction to guided ultrasonic waves and Lamb waves, specifically, will be provided in Section 2. Section 3 will describe the experimental approach to investigating the A0 mode for water sensing including a description of a mockup of a bare fuel cask confinement barrier and the instrumentation used for testing. Section 4 describes the testing performed on the mockup in FY19 and Section 5 describes the next steps and future work. References cited in this document are listed in Section 6.

2. GUIDED ULTRASONIC WAVE SENSING

Guided ultrasonic waves (GUW) involve the introduction of ultrasonic energy with wavelengths on the same order as the dimension of the component under inspection and observing the reflection of that energy from flaws or other discontinuities in the component. Boundary conditions significantly influence the propagation of GUW energy, and the component under inspection may support the propagation of several modes. Each of these modes experience dispersion that can result in significant variation of phase (Vp) and group velocity (Vg) with respect to frequency. Rigorous derivations for propagating GUW modes in several relevant geometries can be found in standard texts, including the text by Rose (1999). For this application, GUW propagation in planar geometry is most relevant and will be described in the remainder of the section.

GUW propagation in planar components can be described using a Cartesian coordinate system and by defining a planar component of thickness b having infinite extent in the x- and y-directions and with surface-normal vectors aligned with the z axis. GUW modes defined as shown in Figure 2-1 are referred to as Lamb waves with wave propagation in the positive x-direction. Lamb waves can consist of an infinite number of symmetric, S_n (n = 0,1,2,…), and anti-symmetric, A_n (n = 0,1,2,…), modes. The nomenclature for these two mode classifications refers to the shape of normal displacement profiles. Illustrations of the lowest order (fundamental) symmetric mode, S0, and lowest order (fundamental) anti-symmetric mode, A0, are provided in Figure 2-2 and Figure 2-3, respectively. These figures display how the A0 and S0 modes have out-of-plane displacements. These out-of-plane displacements occur on both surfaces of the plate and facilitate interaction of the energy in A0 and S0 modes with materials that are intimately coupled to the surfaces of the plate. In this application, the material of interest is liquid water.

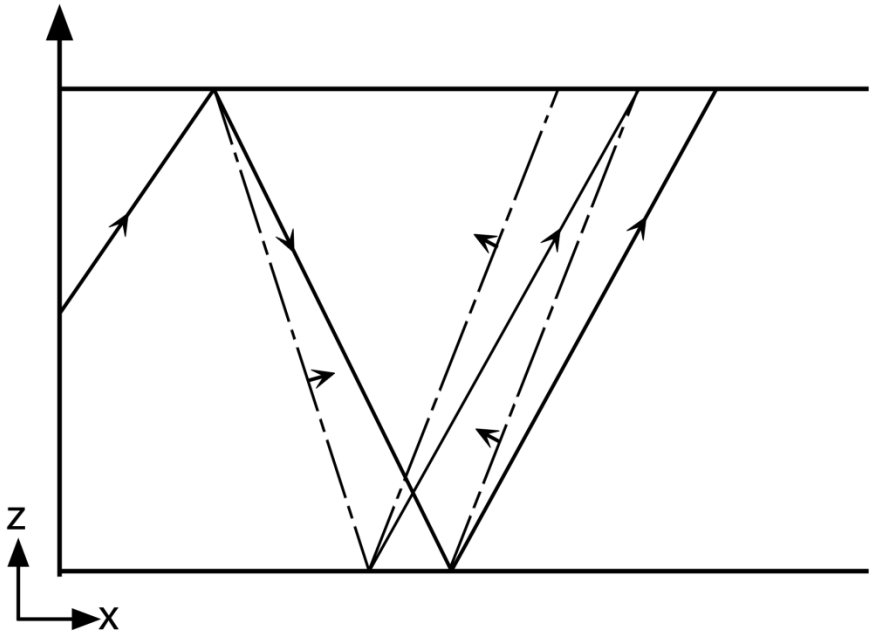

Figure 2-1. Vector Representation of Lamb Wave Propagation Along the x-direction of a Planar Component

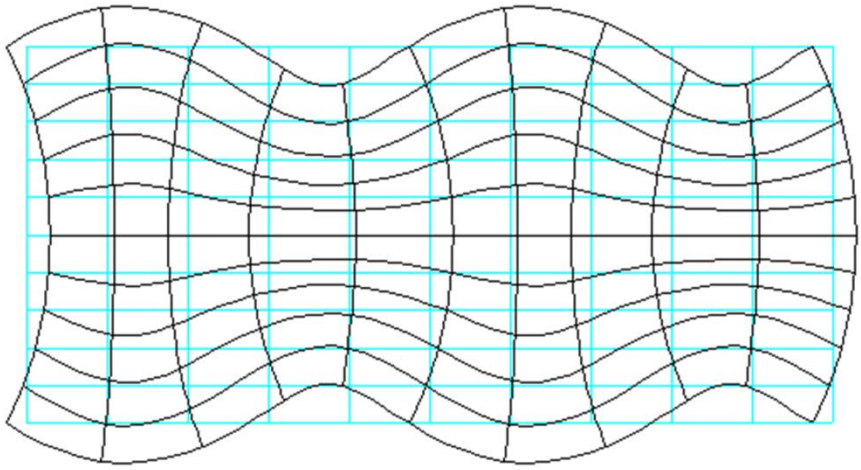

Figure 2-2. Illustration of the Fundamental Symmetric Lamb Wave Mode, S0, Excited in a Planar Component

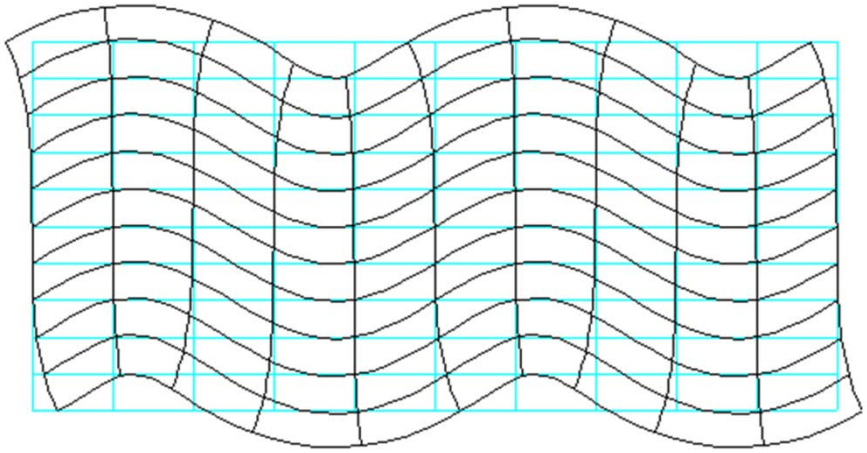

Figure 2-3. Illustration of the Fundamental Anti-Symmetric Lamb Wave Mode, A0, Excited in a Planar Component

Dispersion relationships for the Vg of Lamb waves in a carbon steel plate are shown in Figure 2-4. This plot displays Vg as a function of the product of frequency and component thickness (MHz×mm) and shows that for larger values of this product, more wave propagation modes are supported within the plate including higher-order symmetric and anti-symmetric modes. Having several modes excited within the plate can complicate analyses because the modes can interfere with each other. The shaded area in the left of Figure 2-4 represents the desired region of operation as the minimum number of modes will exist in this regime. Even when operating in this regime, the two fundamental modes, A0 and S0, coexist and can interfere with each other.

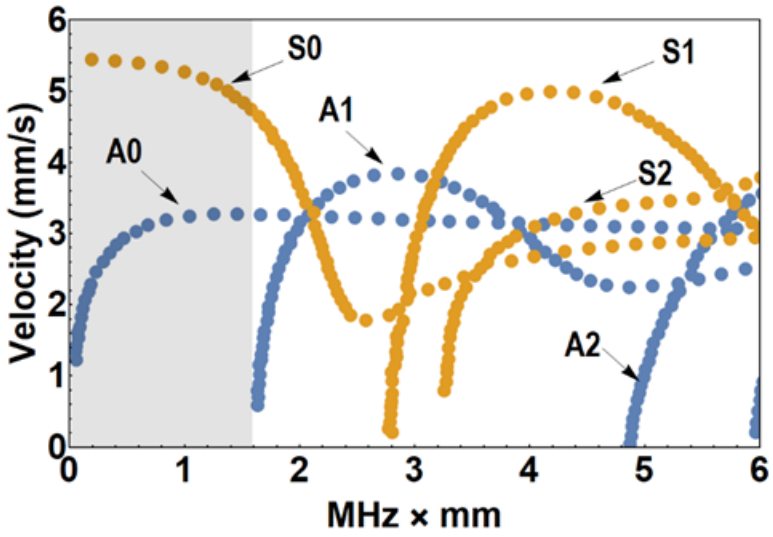

Figure 2-4. Dispersion Relationships for the Group Velocity, Vg, of Lamb Waves Excited in a Planar Component

Interference from coexisting A0 and S0 modes can potentially be mitigated by consideration of Snell's law applied to the refraction of the ultrasonic energy as it crosses a material boundary. Snell's law can be formulated as,

$$c_1 * \sin\theta_2 = c_2 * \sin\theta_1, \quad (1)$$

where c_1 represents the wave speed in medium 1 and c_2 represents the sound speed in medium 2. The angle, θ_1, represents the angle of incidence to the material boundary defined with respect to the normal vector to the plate surface. The angle, θ_2, is the angle at which the signal is directed in medium 2 after passing through the interface. This scenario, for an ultrasonic signal propagated through a Rexolite wedge into a steel plate is illustrated in Figure 2-5. The critical angle, θ_{cr}, can be defined as the angle θ_1 that results in $\theta_2 = 90°$. When the critical angle is reached, the ultrasonic energy is not transmitted into medium 2. This angle can be calculated by the following formula,

$$\theta_1 = \sin^{-1}\frac{c_1}{c_2}. \quad (2)$$

Critical angles for the S0 and A0 modes in steel can be calculated and are tabulated in Table 2-1 for a signal propagated through a Rexolite wedge into steel. Thus, the A0 mode may be isolated from the S0 mode with an incident angle between 31° and 46°. The velocity of sound for Rexolite used in these calculations is 2,325 m/s.

Table 2-1. Tabulation of Critical Angles for the S0 and A0 Modes for Lamb Waves in a Plate for the Shaded Region of Figure 2-4.

	Velocity of sound (m/s)	Critical angles
Steel	~4,500–5,500 (S0)	25° to 31° (Rexolite)
Steel	~3,250 (A0)	~46° (Rexolite)

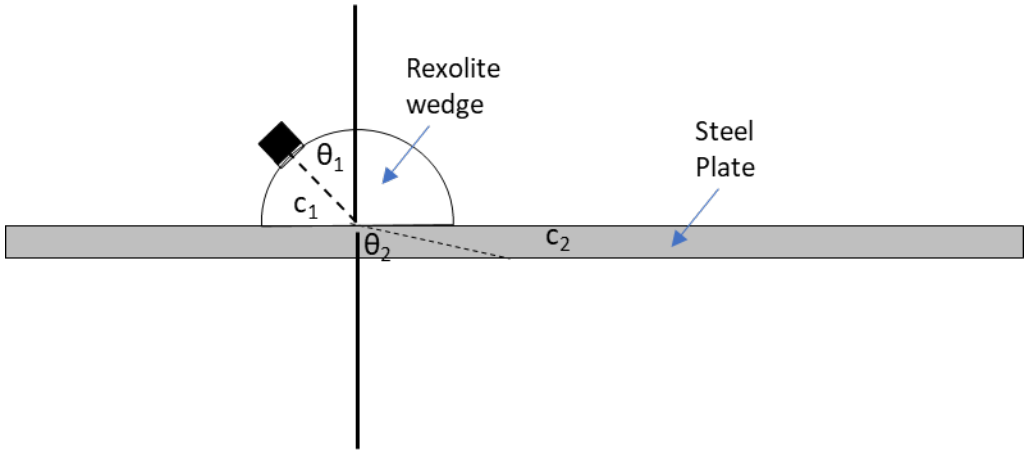

Figure 2-5. Depiction of an Ultrasonic Transducer Attached to a Rexolite Wedge and Mounted on a Steel Plate

3. MOCKUP AND TEST INSTRUMENTATION

This section introduces the reader to test equipment utilized for laboratory studies conducted during FY19. It includes a description of a mockup that was fabricated to facilitate laboratory testing and sensor development and includes a summary of piezocomposite sensors that were used and evaluated in testing. Finally, this section describes a laser vibrometer instrument that was utilized as a receiver and for visualizing the sound field intensity in the mockup.

3.1 Mockup Design and Fabrication

To facilitate testing of ultrasonic sensing of liquid water for relevant geometrical conditions, a mockup was constructed to simulate a portion of the confinement vessel, including portions of the wall and floor, and the path the GUW signals will travel from the accessible exterior surface to the bottom floor of the mockup. A labeled illustration of the mockup is provided in Figure 3-1. The mockup is fabricated from carbon steel material and includes relevant geometrical features. Specifically, the mockup includes a feature labeled the “Flange shoulder.” This feature simulates the flange located at the top of the containment vessel to which transducers will be mounted. The flange is significantly thicker than the wall and bottom of the containment vessel, introducing complexity into the path through which the signals are expected to propagate. Other components, such as the angle supports and support tubing, are not features of the actual cask systems but are incorporated into the mockup for convenience of handling in the laboratory. A photograph of the mockup is provided in Figure 3-2.

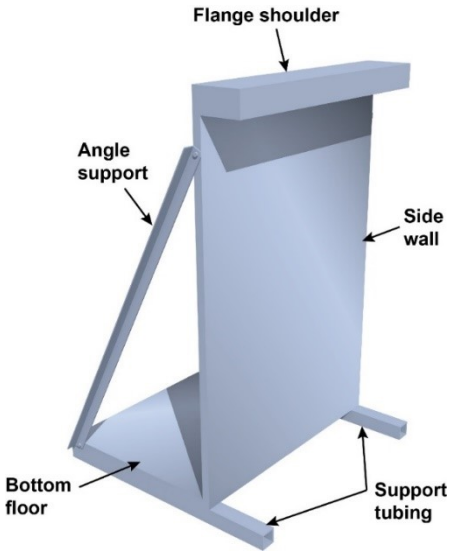

Figure 3-1. Labeled Illustration of Bare Fuel Cask Mockup for Water Sensing Development

Figure 3-2. Photograph of Mockup for Water Sensing Development

3.2 Ultrasonic Transducers

The generation of signals at low frequency is required (~50 kHz) to achieve desired mode generation (minimization of modes higher than A0 and S0) in the mockup side wall and floor. Excitation in this range can be achieved by acquisition of an appropriate transducer with center frequency near 50 kHz or by driving higher-frequency transducers with a low-frequency excitation signal. A transducer is most efficient when driven at its center frequency and it becomes less efficient when driven off its center frequency.

Several in-house (located at Pacific Northwest National Laboratory; PNNL) transducers were identified to begin testing. The transducers all had center frequencies (100 kHz–500 kHz) greater than the targeted 50 kHz. An assessment of these transducers was performed to identify which ones may work best when provided with a low-frequency excitation. This assessment was performed by arranging transmitting and receiving transducers in a through-transmission arrangement and sweeping over a range of excitation frequencies. The results of this assessment are displayed in Figure 3-3. The Olympus V1012 transducer (center frequency at 250 kHz) was included in three transmitter-receiver evaluations: (1) Olympus V1012 – Olympus V1012, (2) Olympus V1011 – Olympus V1012, and (3) GE 389 089 750 – Olympus V1012. Each of these evaluations displays a dip in amplitude at 50 kHz and increasing amplitude with increasing frequency up to 100 kHz. These evaluations also display a peak at 30 kHz–35 kHz. The Olympus V1011 and GE 389 089 750 transducers were paired with the Olympus V1012 transducer because multiple Olympus V1011 and GE 389 089 750 transducers did not exist in-house.

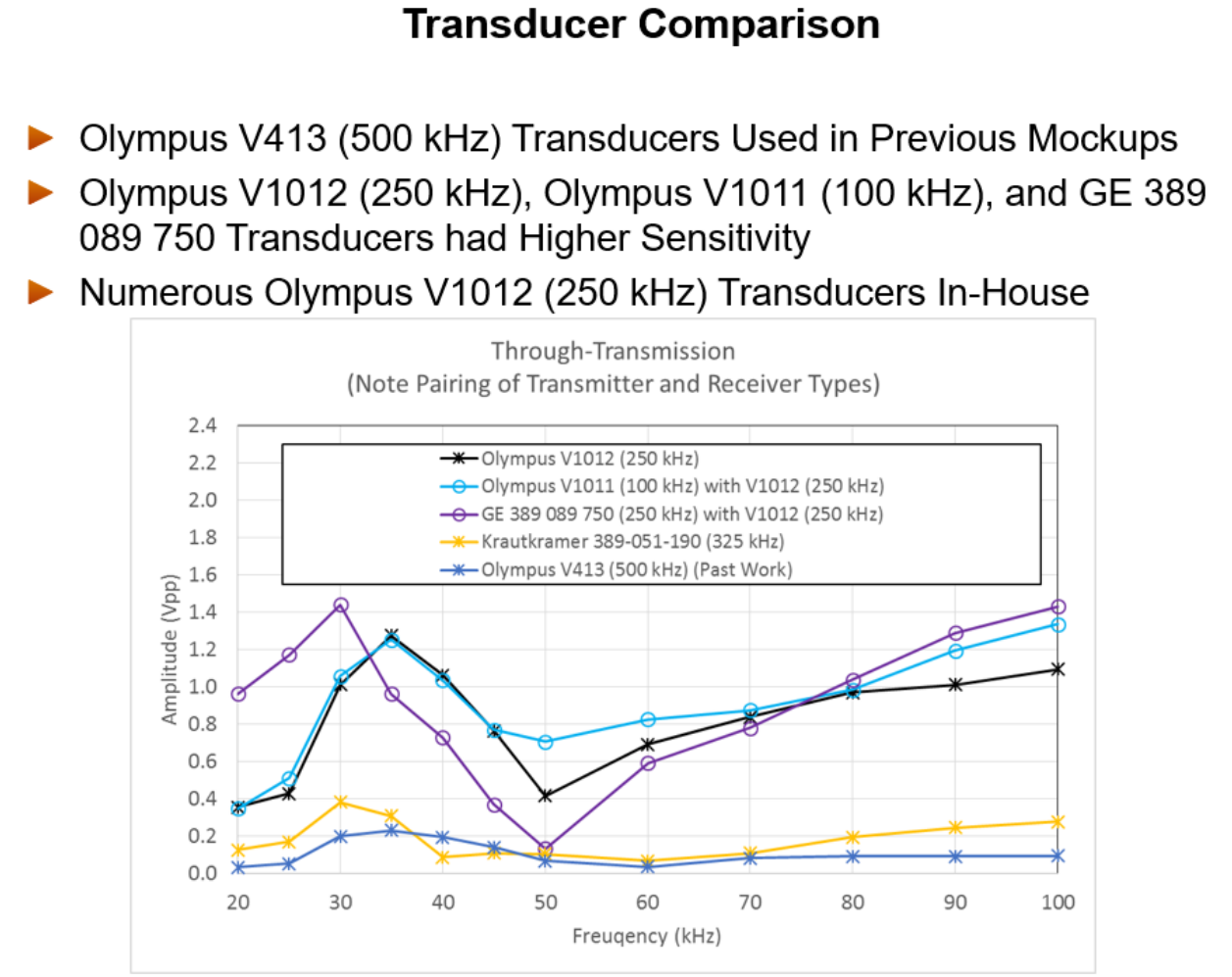

Figure 3-3. Assessment of the Low-Frequency Response of Several In-house (at PNNL) Transducers

In addition to evaluating in-house transducers, PNNL purchased commercially available transducers with nominal 50 kHz center frequency for additional evaluations. Three Olympus X1021 transducers were purchased and three variable angle Rexolite wedges were manufactured. A photograph of the transducers and variable angle wedges is provided in Figure 3-4. The frequency response of the Olympus X1021 transducers was measured and is provided in Figure 3-5. The peak response appears to be near 35 kHz–36 kHz. The strength of the X1021 transducers was also compared to the in-house Olympus V1012 transducers (center frequency of 250 kHz). This comparison is shown in Figure 3-6. The comparison is made to paired V1012 transducers and a V1012 transducer paired with an X1021 transducer. Figure 3-6 demonstrates that the X1021 can provide a response that is orders of magnitude greater than the V1012 transducer in the desired frequency range.

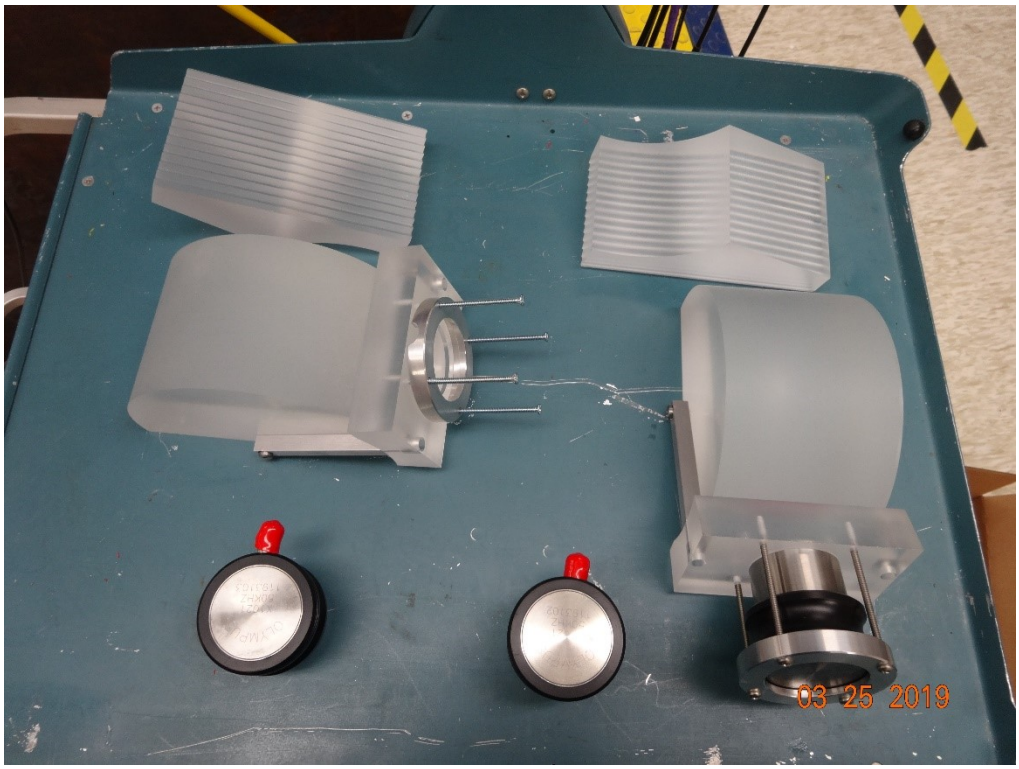

Figure 3-4. Photograph of Olympus X1021 50 Transducers and Variable Angle Rexolite Wedges

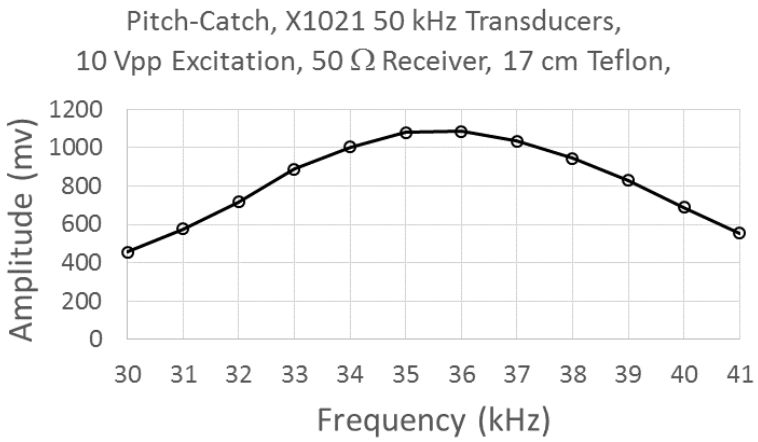

Figure 3-5. Frequency Response of Olympus X1021 nominal 50 kHz Transducers Arranged in a Paired Pitch-Catch Configuration

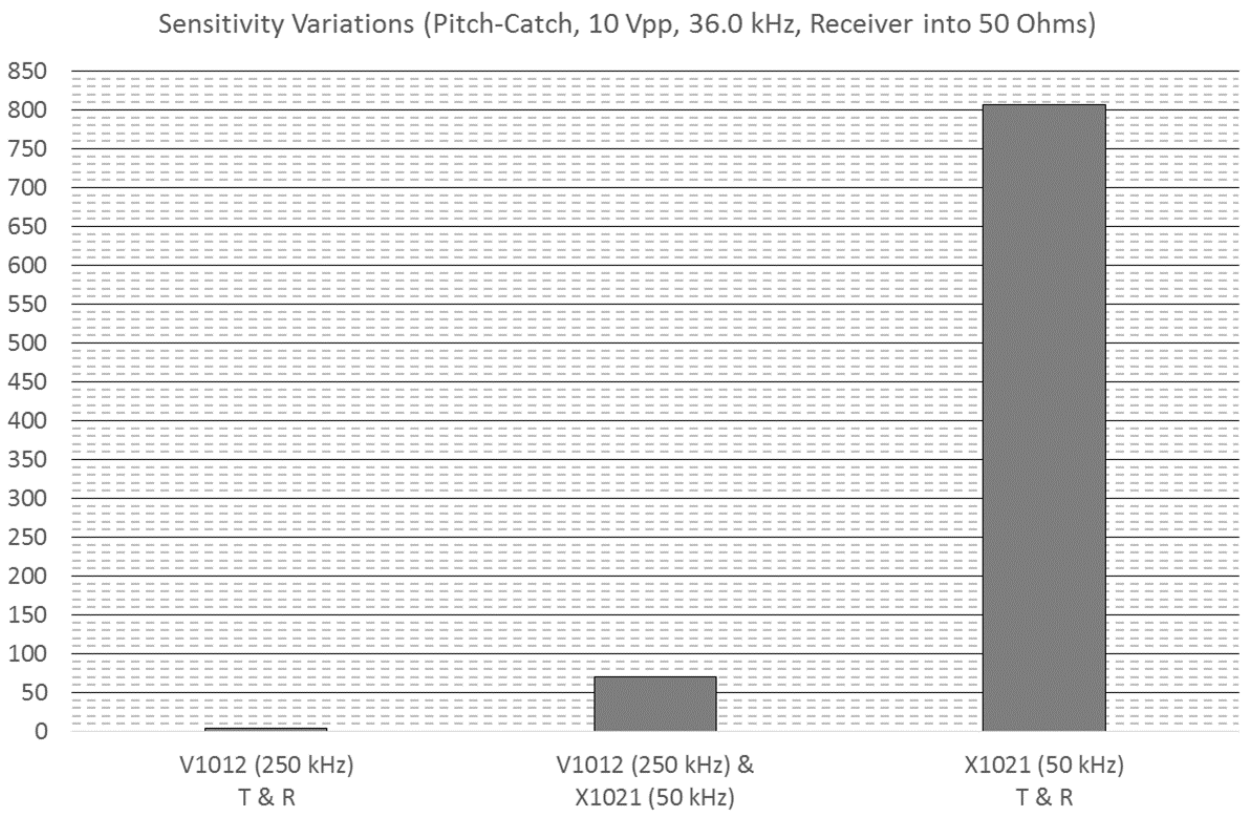

Figure 3-6. Comparison of the Response of the Olympus X1021 Transducer with the Olympus V1012 Transducer

3.3 Laser Vibrometer

Laser Doppler vibrometry (LDV) is a standoff technique for recording the velocity of surface deflections based on optical interferometry. By measuring surface velocity at high sampling rates, vibration characteristics can be easily extrapolated, and this is what supports the majority of vibrometry applications. Vibration can be measured across a very broad bandwidth, from near DC up to several megahertz, and standoff distances can be adjusted from only a few millimeters up to hundreds of meters.

LDV works by launching a laser beam at a surface of interest, as shown in Figure 3-7 (left). The laser beam reflects or scatters from the surface of interest and is recollected by the LDV instrument head. The reflected beam is combined with an unchanging reference beam on a photodetector. The combined beams create interference patterns that change depending on the deflection of the surface. Changes in the interference pattern cause the light intensity at the photodetector to increase or decrease and this measurement will be used to calculate vibration. Usually, the reference arm is also modulated (as by the Bragg cell in the figure) to increase the sensitivity of the measurement and reduce noise. Many different visible and invisible wavelengths of light may be used, but red helium-neon lasers are a common choice.

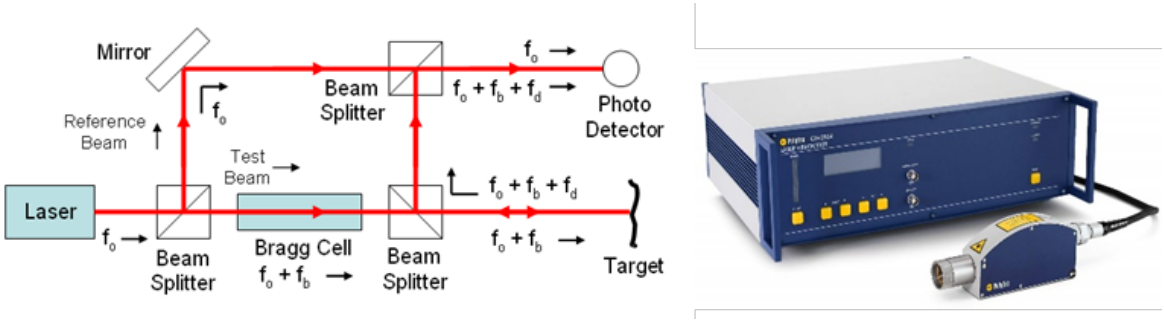

Figure 3-7. Illustration of Basic LDV Function Showing Beam Paths in Red (*left*, source: Wikipedia). Photograph of Commercial Single-Point LDV System Showing Essential Components and Size (*right*, source: Polytec.com).

PNNL has a single-point OFV-5000 laser vibrometer from Polytec Inc. (Figure 3-7, *right*). It uses a red helium-neon laser, has bandwidth up to 2.5 MHz, and can detect surface velocities from vibration up to 25 m/s and surface displacements down to 0.1 pm. The small optical head can be tripod-mounted for convenient positioning. The control unit shown here can be connected to a PC for real-time viewing and saving.

4. SCOPING TESTS

This section describes scoping tests that were performed in FY19 to establish the efficacy of the proposed sensing approach and to establish confidence in the use of the laser vibrometer for visualizing sound field intensity in the mockup. Some of the tests that were performed included testing to confirm the feasibility of generating the desired Lamb wave mode (A0) in the side wall and floor components of the mockup. In addition, some testing was performed to systematically explore propagation of signals through the flange shoulder at the top of the mockup because it is necessary to propagate the energy through the flange shoulder to access the side wall and floor components.

4.1 Confirming Generation of A0 Mode in Wall and Floor of Mockup

Initial testing was performed with in-house Olympus V413 transducers (500 kHz center frequency) to confirm that the desired A0 mode could be generated and propagated through the side wall and floor of the mockup. The receiving and transmitting transducers were mounted on acrylic wedges set to angles above the cutoff for the S0 mode. Three different cases were tested to observe A0 and S0 signal generation and propagation:

- Case 1– Involved transmission and reception over a flat plate portion of the mockup side wall.
- Case 2 – The transmitter and receiver are positioned relative to each other so that a 90-degree bend in the mockup is in the path between the two transducers.
- Case 3 – The transmitter and receiver are positioned in a “quasi pulse-echo” mode so that the signal propagates from the transmitter through the 90-degree bend for two passes (it reflects off the end of the bottom plate) before being received.

A diagram of the instrumentation setup for the three cases is provided in Figure 4-1 and photographs of the transducer positioning for the three cases are provided in Figure 4-2. Results from Cases 1 and 2 are displayed in Figure 4-3. In these A-scans, the approximate arrival times of A0 and S0 modes are indicated. These signals show that the A0 mode is generated for Cases 1 and 2 with minimal S0 mode generation.

The results for Case 3 are displayed in Figure 4-4. The top of the figure displays the A-scan signal obtained on the end of the bottom floor plate of the mockup and the signal shows significant A0 mode with minimal S0 mode contribution. The bottom portion of the figure displays the A-scan signal obtained for the receiver placed in a “quasi pulse-echo” mode. In this case, the transmitter and receiver are both positioned adjacent to each other at the top of the side wall. This arrangement was tested to simulate a pitch-catch arrangement in which a signal is transmitted through the containment vessel with the transmitter and receiver positioned at 180° from each other. The signal appears much more complex as there appear to be contributions from both A0 and S0 modes, and it is likely that reflections from the edges of the plate are contributing to the response. Thus, a limitation of the mockup is the ability to provide a full path for the signal to propagate as would be intended on an actual system. Damping material was applied to the edge of the bottom floor plate (see Case 3 in Figure 4-2) and the signal obtained under this condition was subtracted from the signal obtained with no damping material applied. The difference signal is displayed in red in Figure 4-2. This indicates that the A0 mode dominates the signal with propagation trajectory through the side wall plate and bottom floor plate of the mockup.

In all, the three cases show that the A0 mode can be isolated in the plate sections of the mockup. The geometric limitations of the mockup result in many reflections from the edges of plate sections that complicate the signal that arrives at the receiver in the quasi pulse-echo mode.

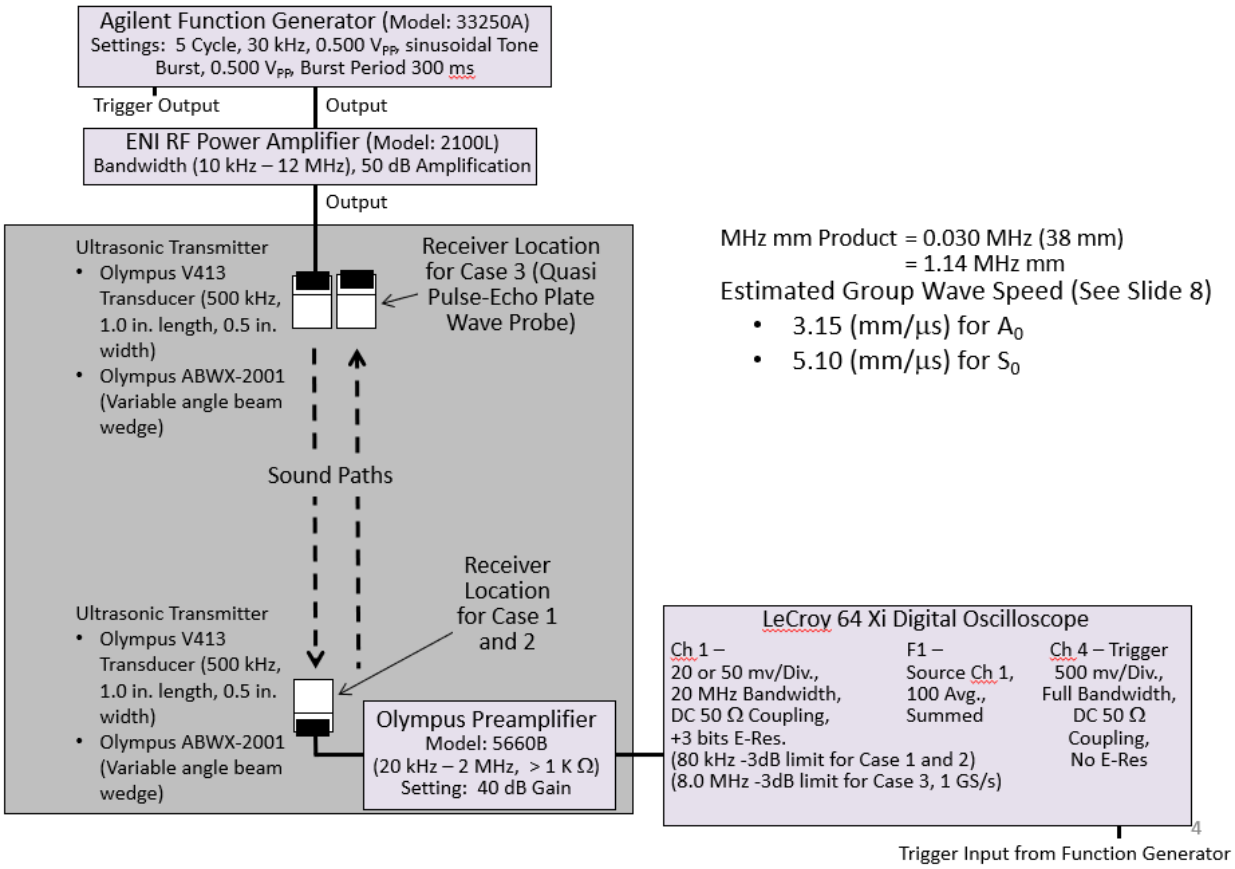

Figure 4-1. Diagram of Instrumentation Setup for Confirming A0 Mode Generation and Propagation for Three Transmitter-Receiver Configurations

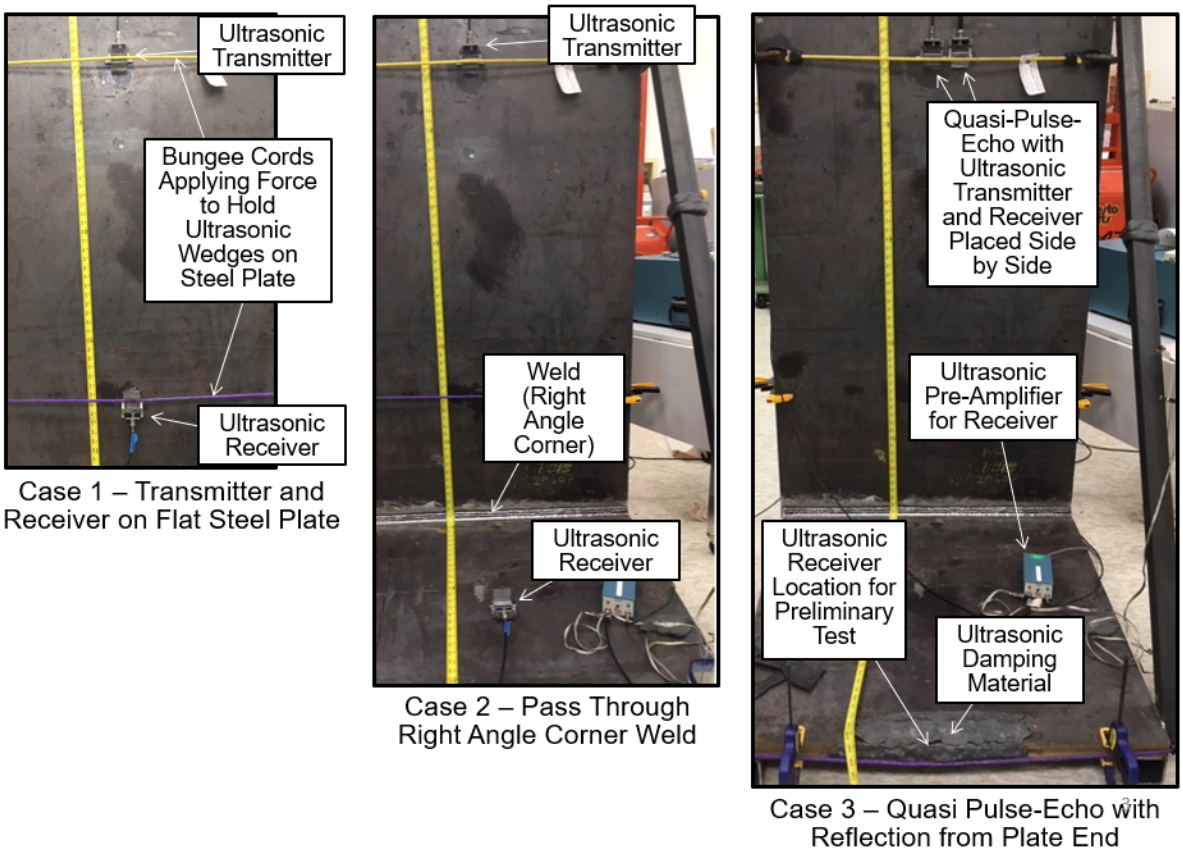

Figure 4-2. Three Cases Studied to Confirm the Propagation of an A0 Signal in the Side Wall and Floor of the Mockup

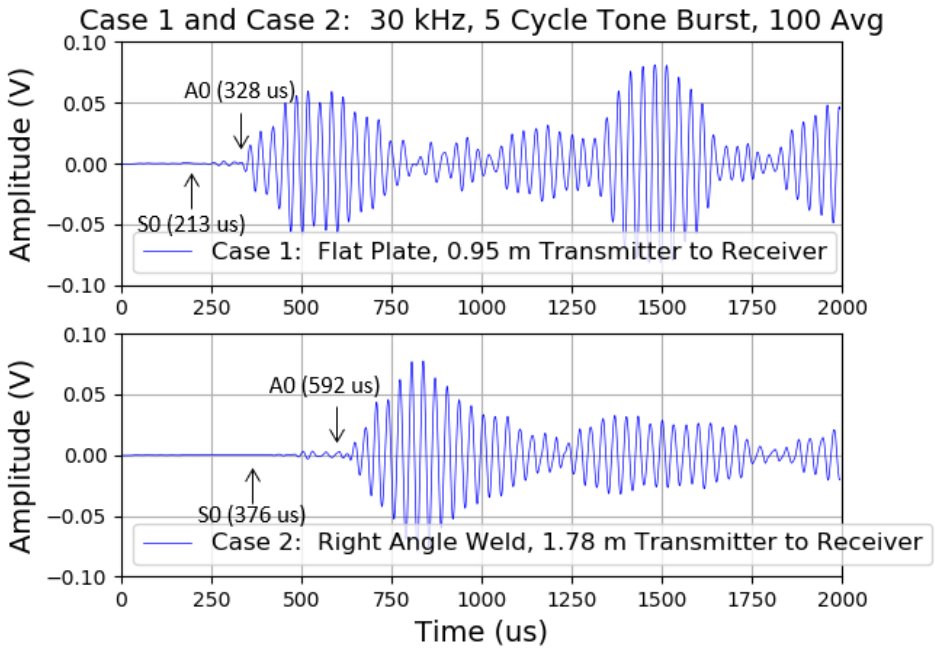

Figure 4-3. Results Obtained from Cases 1 and 2 in Figure 4-2

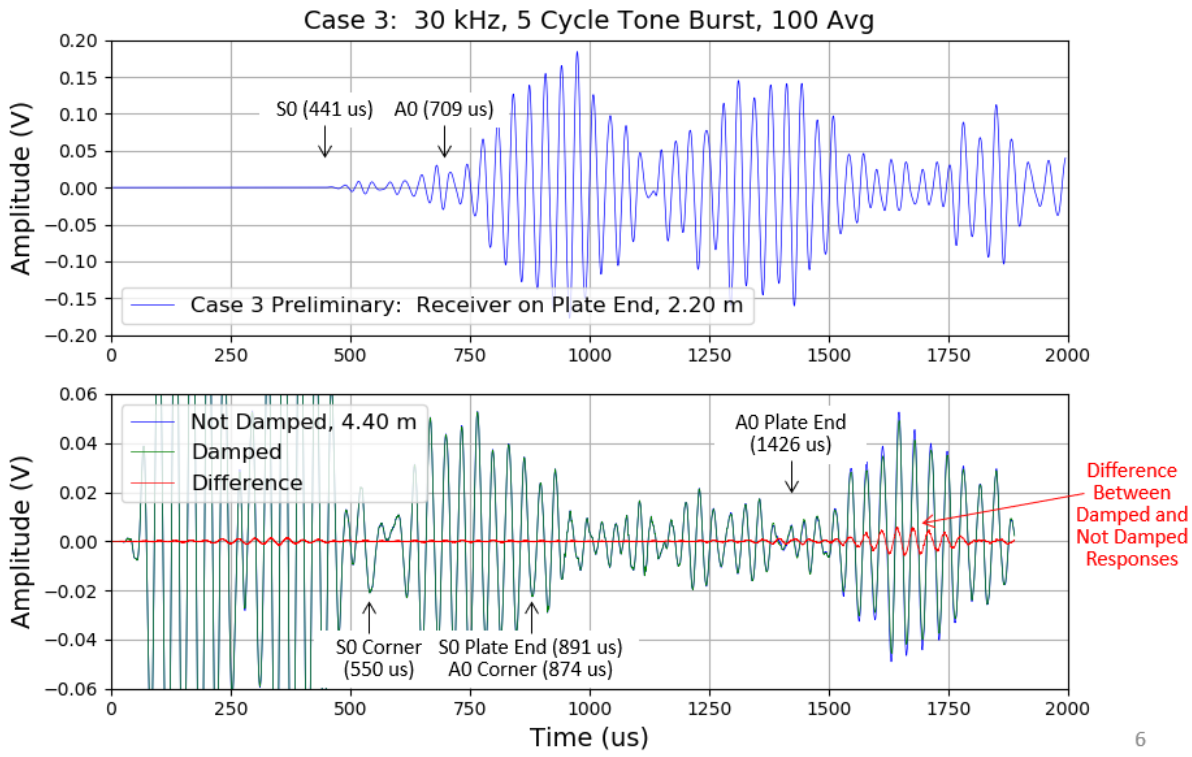

Figure 4-4. Results Obtained from Case 3 in Figure 4-2

4.2 Sound Field Mapping

A grid of laser vibrometer measurements was performed as part of an effort for developing a technique to visualize the sound field in the mockup. The technique is being developed to assess focusing of the sound field in the mockup to inform adjustments to sensor configurations through trial-and-error. Measurements were performed using the laser vibrometer instrument described in Section 3.3. Measurements were collected over an 18 in. × 24 in. grid of points with 3 in. spacing between the points. The measurement grid spanned a portion of the mockup surface with the top right corner (looking into this page) positioned with the center of the transducer and extending to the left 18 in. and extending down by 24 in.

Initial testing was performed with Olympus V413 transducers mounted to variable angle wedges with 50 kHz excitation. Images of the responses are shown in Figure 4-5 displaying the sound field as it emanates from the transmitter oriented near the top of the mockup. In Figure 4-5, the intensity of the sound field is displayed on a spatially discrete set of points and as a continuous field. MATLAB scripts were written for processing and displaying the data and a Hilbert transform was applied to interpolate the sound field intensity between the discrete data points to create the continuous field image. The data in Figure 4-5 is overlaid on a photograph of the mockup.

For this example, the image indicates that the transducer behaves as a point source and provides little focusing to the sound field.

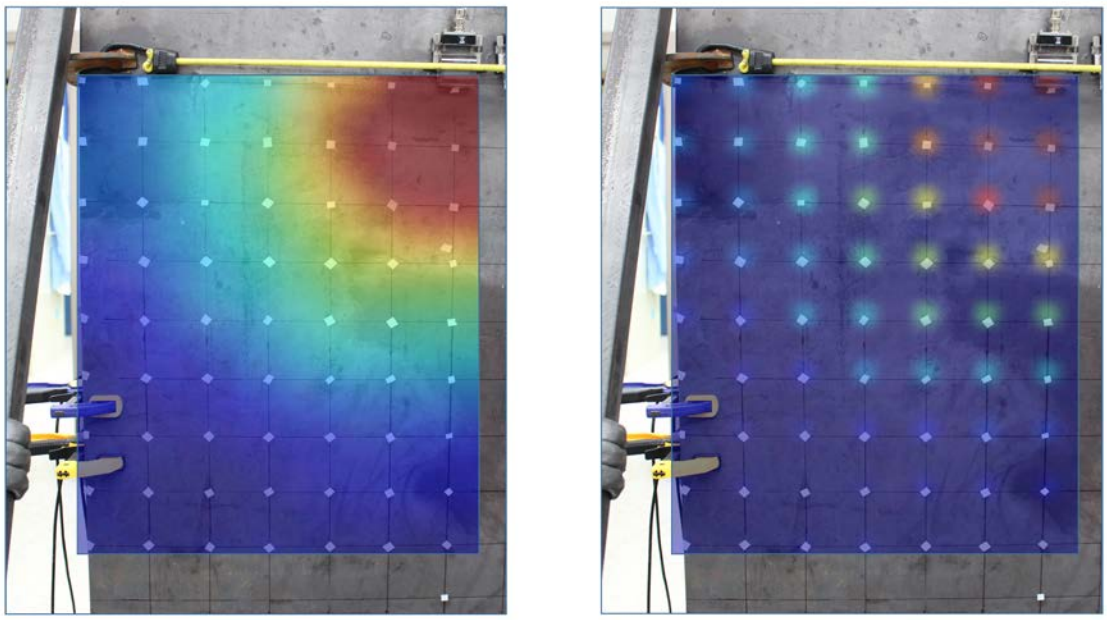

Figure 4-5. Images of the Discrete Laser Vibrometer Measurements of Sound Field Intensity at Grid Points (*right*) and Interpolated Sound Field After Processing by Application of Hilbert Transform (*left*)

Additional testing was performed to verify the laser vibrometer was performing as expected. In this case, the Olympus V413 transducers were excited at 500 kHz. The angle wedges were adjusted to generate surface Rayleigh waves. Maps of the sound field intensity at two points in time are shown in Figure 4-6 and Figure 4-7. Data was collected for the same grid of points as described previously. The image in Figure 4-6 displays a map of the sound field as it is originally excited. Figure 4-7 displays a map of the sound field at 128 microseconds. In this case, it is evident that the energy propagates from the location of the transducer to the bottom of the image. The approximate speed of the Rayleigh wave may be estimated from these images and is approximately 2,500 m/s. The color maps also indicate a region of higher intensity near the top of the image, above the transducer. The pattern of the sound field at this location was inconsistent with a traveling Rayleigh wave and was attributed to noise.

Overall, this test enhanced the confidence that the pattern of the sound field could be accurately characterized with the laser vibrometer.

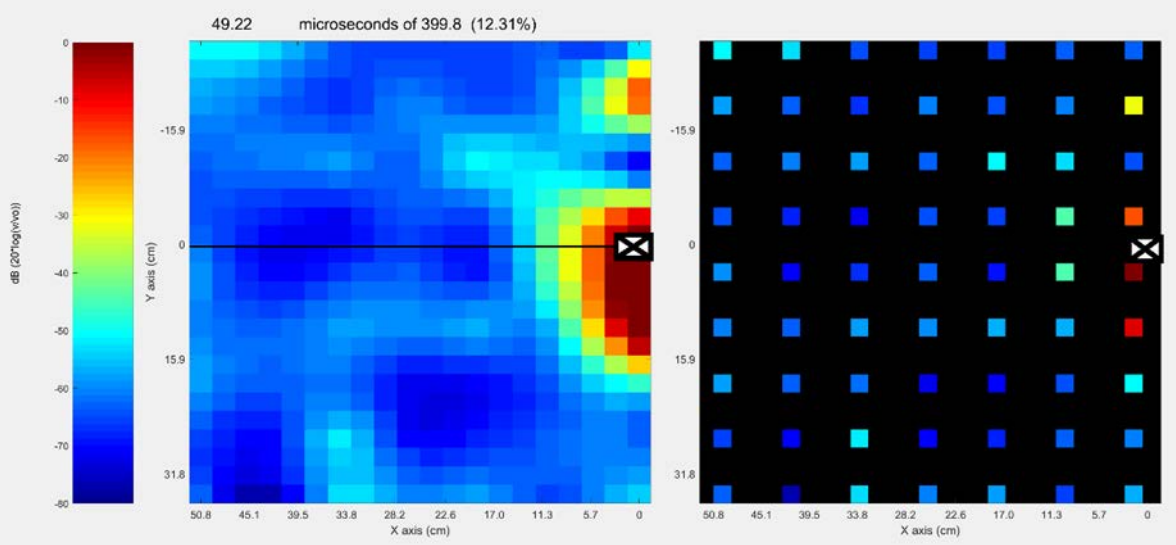

Figure 4-6 Images of the Discrete Laser Vibrometer Measurements of Sound Field Intensity for a 500 kHz Excitation at Grid Points (*right*) and Roughly Interpolated Sound Field After Processing by Application of Hilbert Transform (*left*) at Time 49.22 Microseconds

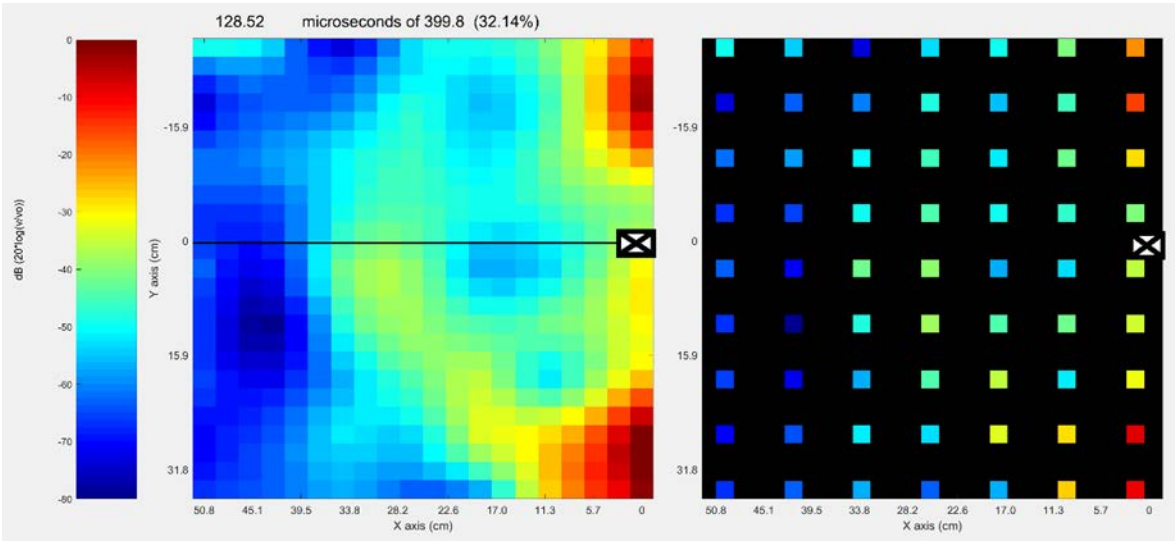

Figure 4-7. Images of the Discrete Laser Vibrometer Measurements of Sound Field Intensity for a 500 kHz Excitation at Grid Points (*right*) and Roughly Interpolated Sound Field After Processing by Application of Hilbert Transform (*left*) at Time 128.52 Microseconds

4.3 Transmitting a Signal Through the Flange Shoulder

The flange shoulder at the top of the mockup represents a transition in material thickness where the flange interfaces with the side wall plate. Although it is demonstrated as possible to generate an A0 mode signal in the side wall and bottom plate with minimal S0 mode interference, the challenge is to introduce the signal to the side wall through the flange shoulder. The behavior of the signal while propagating through the flange shoulder is complex. In this effort, the signal introduced into the side wall plate was systematically analyzed for a single transducer sensor. Specifically, the angle of the transmitter was varied. A depiction of the test setup is displayed in Figure 4-8.

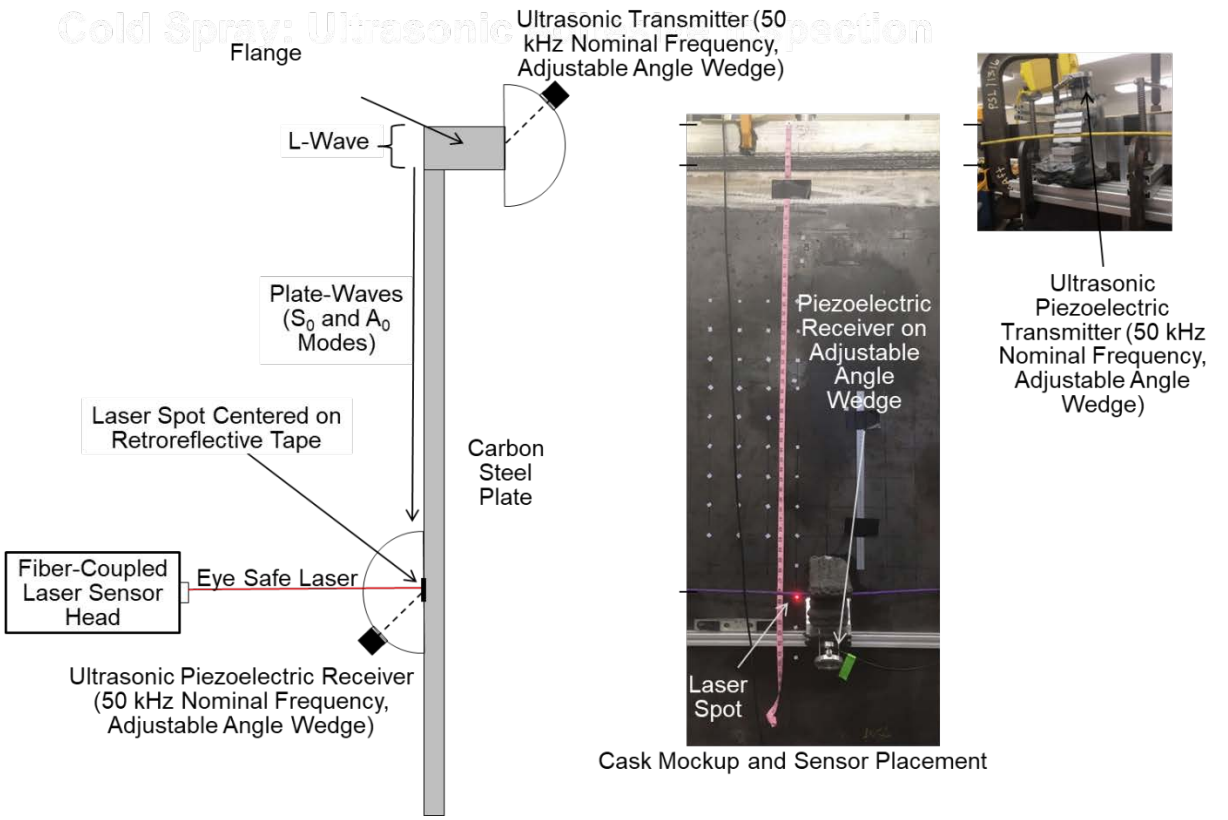

Figure 4-8. Depiction of Setup for Testing the Impact of the Flange Shoulder on Introducing an A0 Signal into the Side Wall of the Cask Mockup

Testing was conducted for several transmitting transducer angles including 0°, 10°, 20°, 30°, 40°, 50°, 60°, and 70°. The receiving transducer angle was maintained at 49°, which was determined to be optimum based on Snell's law analysis. Olympus X1021 transducers were used for both the transmitter and receiver. The laser vibrometer was also used to measure the wavefront generated in the mockup wall next to the receive transducer. Signals obtained at 0° and 70° with the laser vibrometer are shown in Figure 4-9 and Figure 4-10 and signals obtained with the X1021 receiver for 0° and 70° transmitter angles are displayed in Figure 4-11 and Figure 4-12. These figures indicate that the transmitter angle does not appear to have a large influence on the transmission of A0 and S0 modes into the side wall of the mockup. Overall, the signals do indicate that the A0 mode is primarily generated with minimal S0 mode. A-scan signals obtained from the remaining angles (10°, 20°, 30°, 40°, 50°, and 60°) are provided in Appendix B for the laser vibrometer and X1021 receiver.

Additional efforts will focus on mounting the X1021 receiver directly to the flange without the variable angle wedge and adjusting its position (from top to bottom) on the flange surface to observe the efficiency with which A0 mode signals are generated in the side wall.

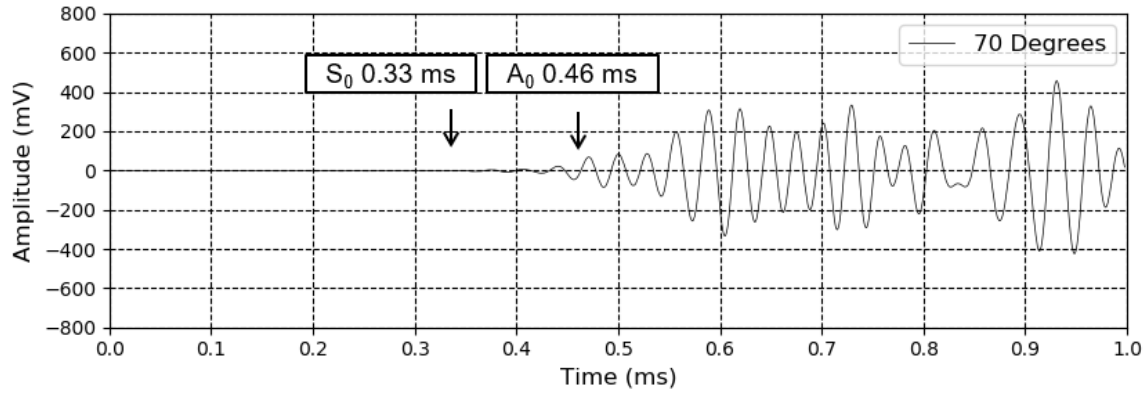

Figure 4-9. A-scan of Laser Vibrometer Response with the Estimated Arrival Times of the S0 and A0 Signals Labeled for Transmitter Angle of 70°

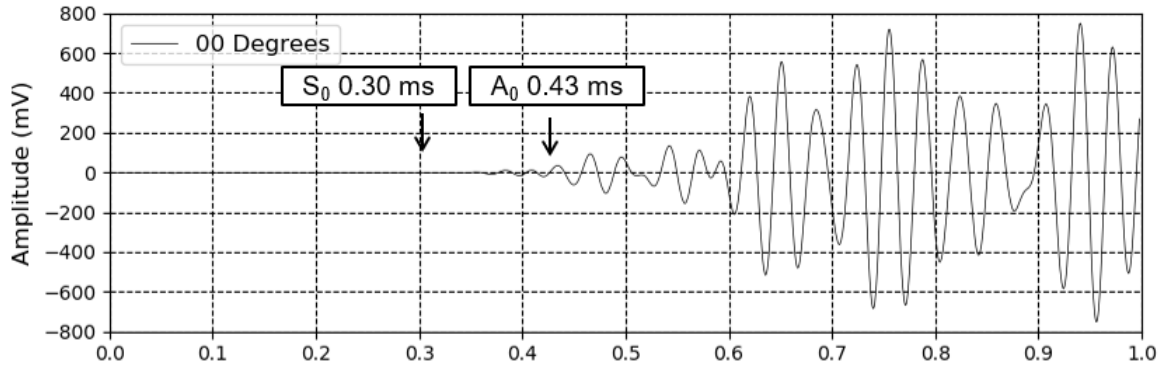

Figure 4-10. A-scan of Laser Vibrometer Response with the Estimated Arrival Times of the S0 and A0 Signals Labeled for Transmitter Angle of 0°

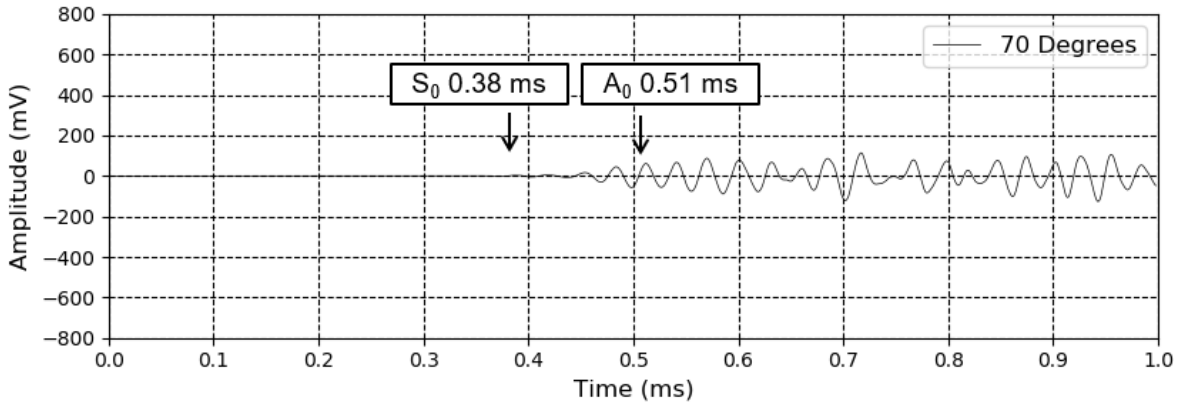

Figure 4-11. A-scan of Piezoelectric Receiver Response with the Estimated Arrival Times of the S0 and A0 Signals Labeled for Transmitter angle of 70°

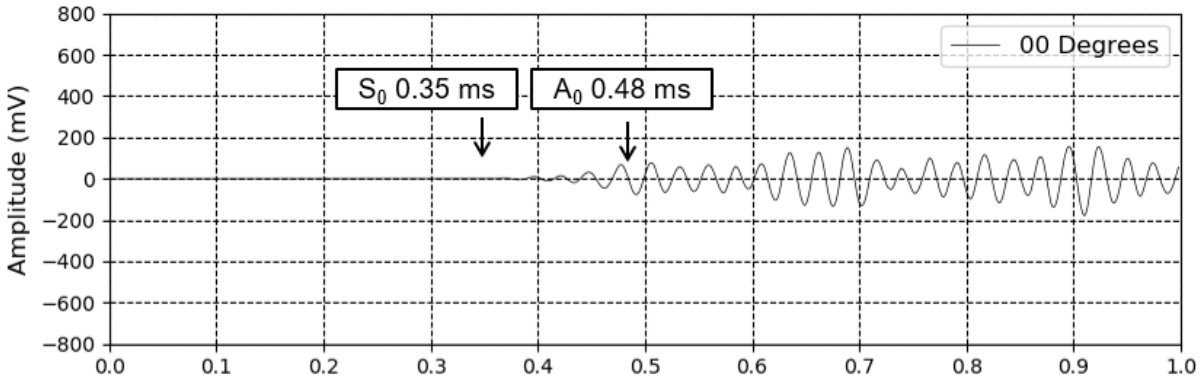

Figure 4-12. A-scan of Piezoelectric Receiver Response with the Estimated Arrival Times of the S0 and A0 Signals Labeled for Transmitter Angle of 0°

This page is intentionally left blank.

5. PATH FORWARD

As noted in the introduction, the overall approach to developing the sensor technology is experimental and is focused on optimizing the A0 mode energy that gets coupled into the wall and floor components of the mockup and then exploring the sensitivity of the A0 mode to quantities of water on the floor. Scoping work was performed in FY19 to identify design parameters for an eventual prototype. The flange shoulder at the top of the mockup introduces a complexity with respect to generating desired modes in the side wall and floor of the mockup and ensuring minimal excitation of unwanted modes. A systematic evaluation of the angle of incidence for transducers mounted on the exterior face of the flange shoulder has been performed with the receiver mounted on the vertical side wall of the mockup. A similar evaluation is planned to continue into FY20 with the receiver mounted on the floor of the mockup to assess coupling of the A0 mode into the floor component.

Additionally, testing will be performed in FY20 to explore multiple transducer array configurations and to investigate the ability to manipulate focusing of the sound field by varying practical sensor parameters (i.e., number, spacing, and geometric arrangement of transducers). The results of this testing will inform the design of a prototype sensor.

Evaluating the sensitivity of the A0 mode to quantities of water on the floor of the mockup will also be investigated once a prototype sensor design has been established. In this phase of testing, liquid water will be introduced to the floor of the mockup and the impact on the A0 mode signal as a function of water quantity will be observed and analyzed.

Although the current mockup simulates many relevant features for this application, it introduces edge effects that will not be present in actual systems. A true pitch-catch configuration with a transmitter and receiver mounted on the exterior face of the flange but located on opposite sides of the DSS (positioned 180° relative to each other) cannot be tested with this mockup. Once suitable design parameters for a prototype sensor are determined, testing on a full-scale system will be useful.

This page is intentionally left blank.

6. REFERENCES

Jung H, P Shukla, T Ahn, L Tipton, K Das, X He and D Basu. 2013. *Extended Storage and Transportation: Evaluation of Drying Adequacy* San Antonio, TX: Center for Nuclear Waste Regulatory Analyses. ADAMS Accession No. ML13169A039.

Knoll RW and ER Gilbert. 1987. *Evaluation of Cover Gas Impurities and Their Effects on the Dry Storage of LWR Spent Fuel*. PNL-6365. Richland, WA: Pacific Northwest Laboratory.

Rose JL. 1999. *Ultrasonic Waves in Solid Media*, Cambridge, United Kingdom: Cambridge University Press.

Salazar A, RJM Pulido, ER Lindgren and SG Durbin. 2019. *Advanced Concepts for Dry Storage Cask Thermal-Hydraulic Testing.* SAND2019-XXXX R. Albuquerque, NM: Sandia National Laboratories.

This page is intentionally left blank.

APPENDIX A

QNDE2019 EXTENDED ABSTRACT

46th Annual Review of Progress
in Quantitative Nondestructive Evaluation
QNDE2019
July 14-19, 2019, Portland, OR, USA

QNDE2019-1234

LIQUID WATER SENSING IN DRY CASK STORAGE SYSTEMS BY GUIDED WAVES

Ryan M. Meyer[1], Morris S. Good, Jonathan D. Suter, Francesco Luzi, Bill Glass, Chris Hutchinson
Pacific Northwest National Laboratory (PNNL)
Richland, WA

ABSTRACT

This work focuses on a method for detecting liquid water inside of dry cask storage systems (DCSSs). Ideally, the environment inside of a DCSS confinement is inert and free of water to prevent potential corrosion of used fuel cladding or other internal hardware. However, there is some uncertainty about the amount of residual water potentially left behind in a DCSS after drying processes. Considering the complex spatial and time-dependent temperature profiles in dry storage casks, water may be in liquid or gas phase depending on location inside of the cask and how long the cask has been in storage. This paper describes development of an ultrasonic technique for sensing liquid water inside a Transnuclear TN-32 DCSS. This system is being used in a demonstration of the efficacy of dry storage of high burnup fuel in DCSSs in collaboration between the United States nuclear power industry and the United States Department of Energy.

Keywords: ultrasound, fluid detection, dry cask storage

1. INTROD1UCTION

This work focuses on a method for detecting and measuring water inside of dry cask storage systems (DCSSs) via sensors mounted exterior to the confinement boundary and requiring no physical penetration of the confinement boundary. Ideally, the environment inside of a DCSS confinement is inert and free of water to prevent potential corrosion of used fuel cladding or other internal hardware. However, there is some uncertainty about the amount of residual water potentially left behind in a DCSS after drying processes. Considering the complex spatial and time-dependent temperature profiles in dry storage casks, water may be in liquid or gas phase depending on location in the cask and how long the cask has been in storage. A review of drying specifications by several vendors concludes that if the specifications are followed correctly, the residual moisture left behind in DCSSs should present an insignificant risk to cladding degradation [1]. A more recent analysis has concluded that much larger quantities of residual water could remain in DCSSs, but the amount would still not be expected to lead to significant corrosion of fuel cladding or other internal components [2]. The assumptions made regarding the possible quantities of residual water or their potential significance have not yet been corroborated with field experience for periods of extended storage. The measurement techniques described here can facilitate the direct observation of residual water in the field and help establish operational data that can inform operating and licensing decisions for extended periods of storage.

This paper describes development of an ultrasonic technique for sensing liquid water inside of a Transnuclear TN-32 DCSS. This system is being used in a demonstration of the efficacy of dry storage of high burnup fuel in DCSSs in collaboration between the United States nuclear power industry and the United States Department of Energy.

2. BACKGROUND

The transfer of spent fuel into DCSS systems occurs in the spent fuel pool facility of nuclear power plants (NPPs). The process involves submerging the opened DCSS system into the pool and loading the spent fuel under water to minimize worker exposure to radiation. Once loaded, a lid is placed on the DCSS system and it is lifted out of the spent fuel pool. After removal from the spent fuel pool, the DCSS is drained and undergoes a drying procedure to remove water that is not discharged by draining. Eventually, the system is sealed and backfilled with an inert buffer gas (such as He) to protect the fuel cladding from corrosion.

The Transnuclear TN-32 DCSS can be referred to as a bare fuel loaded system [3]. Used fuel is loaded into a fuel basket inside of a metal confinement boundary, which is integrated with additional layers of materials for biological shielding and physical protection. An illustration of the TN-32 DCSS is provided in Figure 1. The figure shows the layered design of the system, and the interfaces between these layers prevent the efficient transmission of ultrasonic signals to the interior. One potential path for transmitted ultrasound from the exterior of the

[1] Contact author: Ryan.Meyer@pnnl.gov

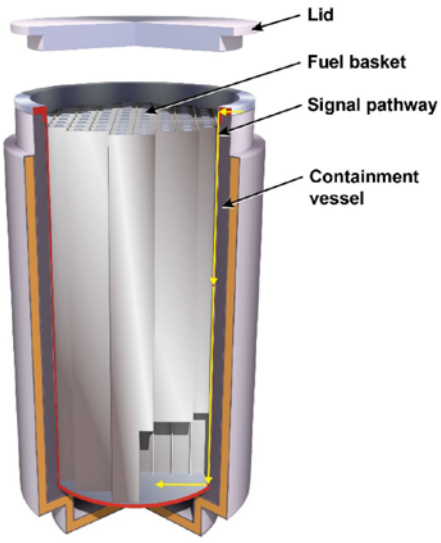

FIGURE 1: REPRESENTATION OF TN-32 DSS SYSTEM ILLUSTRATING PATH FOR ULTRASONIC SIGNAL TO INTERIOR.

DCSS to the interior is through the path identified in Figure 1. The figure illustrates the inner confinement barrier with a cup-like configuration that expands into a flange at the top end. The outer layers for biological shielding and physical protection wrap around the confinement barrier but only extend up to the underside of the shoulder formed by the flange of the confinement barrier. Thus, the outer face of the confinement barrier flange is directly accessible from the DCSS exterior and enables the transmission of ultrasonic signals to the cask interior.

3. APPROACH

The approach for sensing water at the bottom of the confinement barrier is based on transmission of ultrasonic energy from sensors mounted on the exterior-facing surface of the confinement barrier flange. To do this, it is proposed to generate guided ultrasonic plate waves in the confinement barrier wall. More specifically, the approach is based on the generation of the fundamental anti-symmetric plate wave mode, A0. Background information on plate waves and specific excitation modes can be found in ultrasonic textbooks [4]. Dispersion curves for the group velocity in this geometry are displayed in Figure 2. The shaded area to the left of the figure represents the desired region of operation as the minimum number of modes will exist in this regime. For this application, operating at frequencies less than 100 kHz is required. Even when operating in this regime, it is possible for S0 modes to exist and complicate signal interpretation.

3.1 Mockup

A mockup for developing the ultrasonic sensing method for detecting liquid water at the bottom of the DCSS was designed

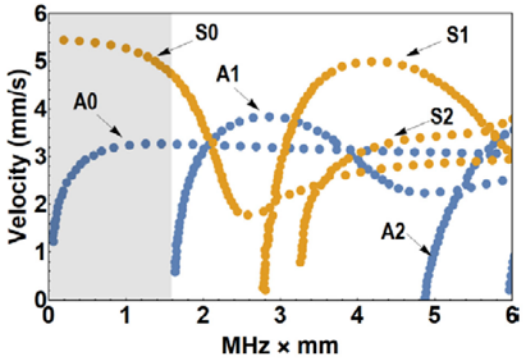

FIGURE 2: DISPERSION CURVES FOR GROUP VELOCITIES OF ANTISYMMETRIC AND SYMETRIC PLATE MODES.

and fabricated. The mockup was designed to capture relevant dimensions and geometric features and to simulate the access path for ultrasonic signals from the exterior surface to the interior, as shown in Figure 1. A drawing of the mock-up is provided in Figure 3, which shows that the curvature of the confinement barrier sidewall is neglected. This approximation is justified as the radius of curvature for the wall is much greater than the wall thickness. The mockup is fabricated from carbon steel material.

3.2 Scoping Tests and Equipment

Scoping tests are currently being performed to optimize sensor design. The flange at the top of the confinement barrier represents a geometric complexity which is expected to make the transmission of A0 modes though the confinement barrier sidewall more challenging. The angle of incidence for

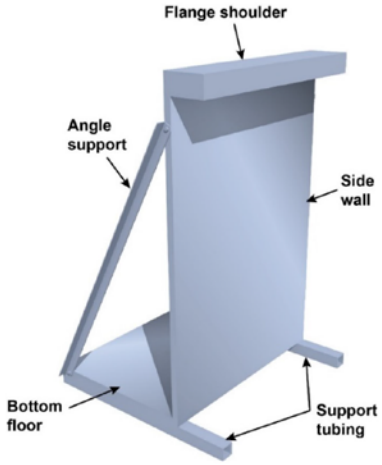

FIGURE 3: ILLUSTRATION OF MOCKUP TO SIMULATE SIGNAL PATH ON TN-32 DSS.

transducers mounted on the exterior face of the flange will impact the efficiency with which ultrasonic energy that enters through the flange will convert to A0 mode and propagate through the side wall.

In this effort, the optimum angle of incidence will be evaluated empirically using commercial off-the-shelf piezoelectric transducers and a variable angle wedge. The angle of incidence will be systematically varied while the strength of the A0 signal that propagates through the mockup sidewall is recorded.

Transducer array configurations will also be explored to improve control of sound field focusing and directionality in the confinement barrier wall. To observe the sound field in the mockup, a laser interferometer is set up and scanned over a grid of points. The spatial distribution of the sound field intensity of signals leaving the transmitter can be mapped for visual presentation. A photograph of the mockup and measurement equipment is provided in Figure 4.

4. RESULTS

Testing has been performed to confirm that the A0 mode can be generated with enough isolation (i.e., with little interference from the S0 mode) in the vertical plate portion of the mockup. Additional testing was performed so that the A0 mode could be propagated through the 90° joint connecting the vertical plate to the horizontal plate at the bottom of the mockup. In this case, testing was performed to assess the impact of the 90° joint on the A0 signal considering 1 pass and 2 passes through the joint. These tests are referred to as Cases 1, 2, and 3:

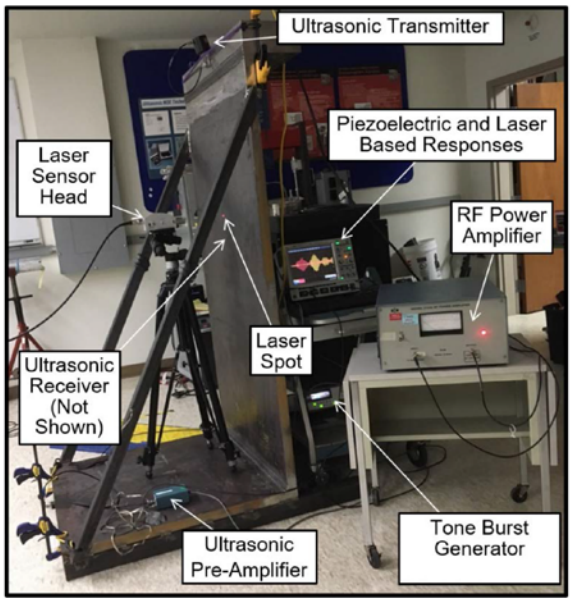

FIGURE 4: PHOTOGRAPH OF MOCKUP AND MEASUREMENT AND TEST EQUIPMENT.

- Case 1 – Generation of A0 mode in vertical plate of mockup (transmitter and receiver on vertical plate)
- Case 2 – Propagation of A0 mode through 1 pass through 90° joint (transmitter on vertical plate; receiver on bottom plate)
- Case 3 – Propagation of A0 mode through 2 passes through 90° joint (transmitter and receiver co-located near top of vertical plate

A-scan responses for Cases 1 and 2 are displayed in Figure 5 while the A-scan response for Case 3 is provided in Figure 6. Figure 5 confirms that an A0 mode signal can be generated and propagated through the 90° joint without significant interference from the S0 mode. Figure 6 depicts a more complicated signal. In this case, it appears that the receiver is picking up several reflections from the mockup boundaries. Damping material was placed on the end edge of the bottom mockup plate, and the resulting signal was subtracted from the signal obtained without application of the damping material. The "Difference" response in Figure 6 is obtained from this subtraction. The response shows that only the A0 mode is propagating to the end of the bottom plate and back to the receiver.

Finally, a map of the sound field intensity in the mockup measured with the laser interferometer is shown in Figure 7. The right side of the figure displays the intensity on the discrete grid points (3 in. × 3 in.) where measurements were collected. A Hilbert transform is applied to generate a continuous map of the intensity on the left. Significant divergence of the sound field can be observed for the single transducer transmitter.

5. FUTURE WORK

Further scoping work will be performed to determine suitable parameters for a prototype sensor. Current testing has focused on verifying the generation of the A0 mode in the plate components of the mockup and verify that passes through 90° joints are feasible with minimal degradation of the A0 signal.

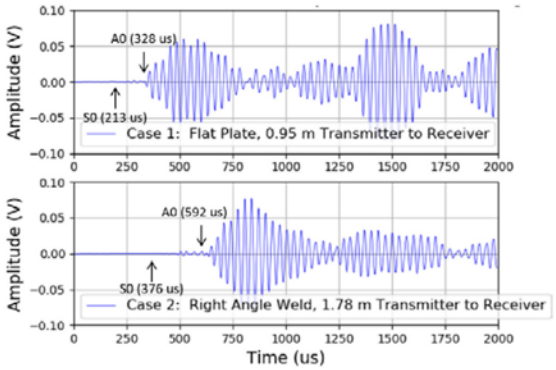

FIGURE 5: A-SCAN RESPONSES FOR (TOP) CASE 1– GENERATION OF A0 MODE IN VERTICAL PLATE OF MOCKUP AND (BOTTOM) CASE 2 – PROPAGATION OF A0 MODE THROUGH 1 PASS THROUGH 90° JOINT (TRANSMITTER ON VERTICAL PLATE; RECEIVER ON BOTTOM PLATE)

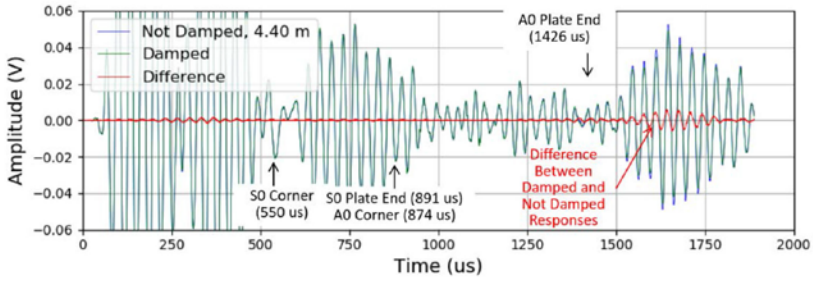

FIGURE 6: A-SCAN RESPONSES FOR CASE 3– - PROPAGATION OF A0 MODE THROUGH 2 PASSES THROUGH 90° JOINT

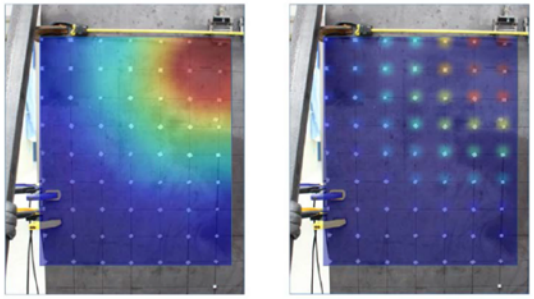

FIGURE 7: INTENSITY MAPS OBTAINED WITH THE LASER VIBROMETER: (RIGHT) REPRESENTATION OF INTENSITY AT DISCRETE GRID MEASUREMENT POINTS, (LEFT) CONTINUOUS REPRESENTATION AFTER PROCESSING ORIGINAL DATA.

The flange shoulder at the top of the mockup introduces a complexity with respect to generating desired modes and ensuring minimal excitation of unwanted modes. A systematic evaluation of angle of incidence for transducers mounted on the exterior face of the flange shoulder will be performed. In addition, multiple transducer array configurations will be investigated to improve focusing of the energy.

Although the current mockup simulates many relevant features for this application, it introduces edge effects that will not be present in actual systems. Further, a true pitch-catch configuration with a transmitter and receiver mounted on the exterior face of the flange but located on opposite sides of the DSS (positioned 180° relative to each other) can not be tested with this mockup. Once suitable design parameters for a prototype sensor are determined, testing on a full-scale system will be useful.

ACKNOWLEDGEMENTS

This work was funded by the U.S. Department of Energy (DOE) Spent Fuel & Waste Science Technology program and performed at PNNL. PNNL is a multi-program national laboratory operated by Battelle Memorial Institute for the U.S. DOE under DE-AC06-76RLO 1830.

REFERENCES

[1] Knoll, R W and Gilbert, E R. "Evaluation of Cover Gas Impurities and Their Effects on the Dry Storage of LWR Spent Fuel." PNL-6365. Pacific Northwest Laboratory, Richland, WA. 1987.

[2] Jung, Hundal; Shukla, Pavan; Ahn, Tae; Tipton, Lynn; Das, Kaushik; He, Xihua; and Basu, Debashis. "Extended Storage and Transportation: Evaluation of Drying Adequacy ". Center for Nuclear Waste Regulatory Analyses, San Antonio, TX. 2013.

[3] Hanson, Brady D; Alsaed, Halim; Stockman, Christine; Enos, David; Meyer, Ryan M; and Sorenson, Ken. "Used Fuel Disposition Campaign - Gap Analysis to Support Extended Storage of Used Nuclear Fuel, Rev. 0." FCRD-USED-2011-000136 Rev. 0, PNNL-20509. U.S. Department of Energy, Washington, D.C. 2012.

[4] Cheeke, J. David N. *Fundamentals and Applications of Ultrasonic Waves*. CRC Press, Boca Raton, FL (2002).

This page is intentionally left blank.

APPENDIX B
–
A-SCAN RESPONSES FOR EVALUATION OF TRANSMISSION THROUGH THE MOCKUP FLANGE

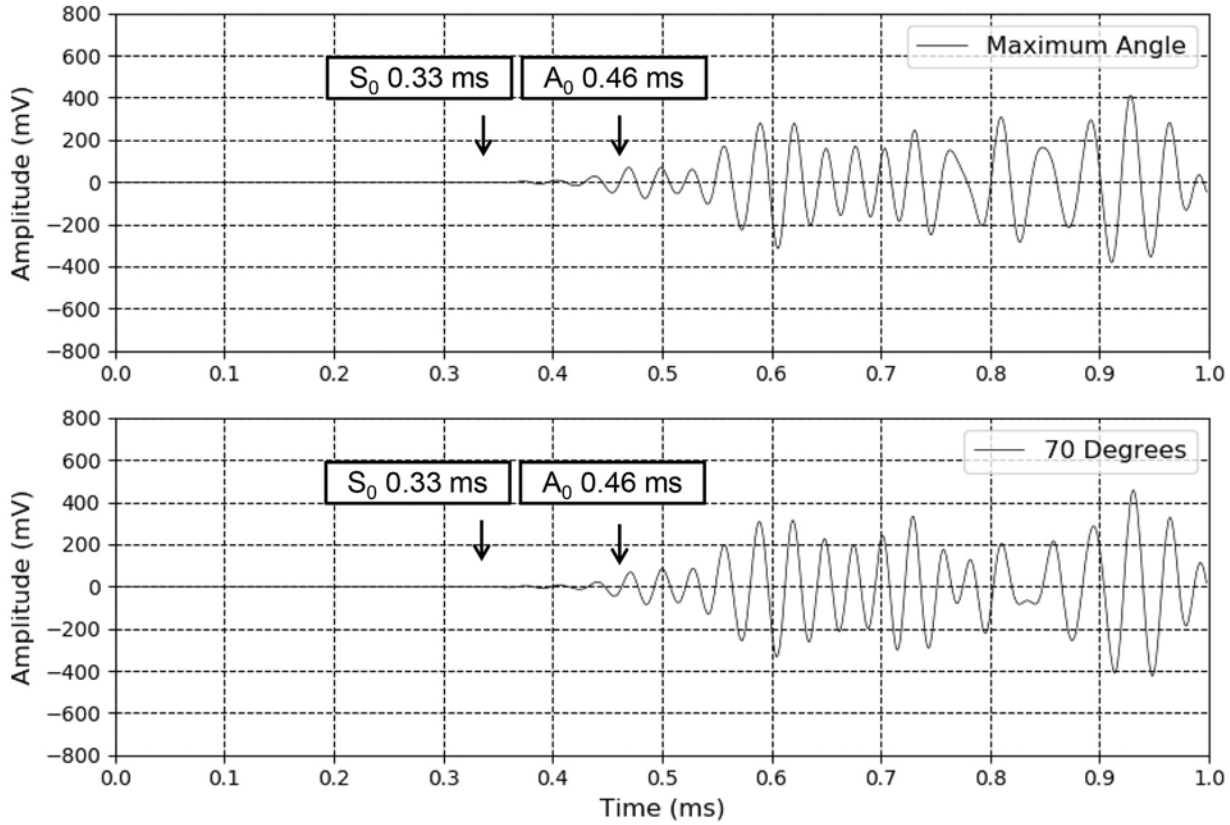

Figure B-1. A-scan of Laser Vibrometer Response with the Estimated Arrival Times of the S0 and A0 Signals Labeled for Transmitter Angle of 70° (*bottom*) and the Maximum Angle (*top*)

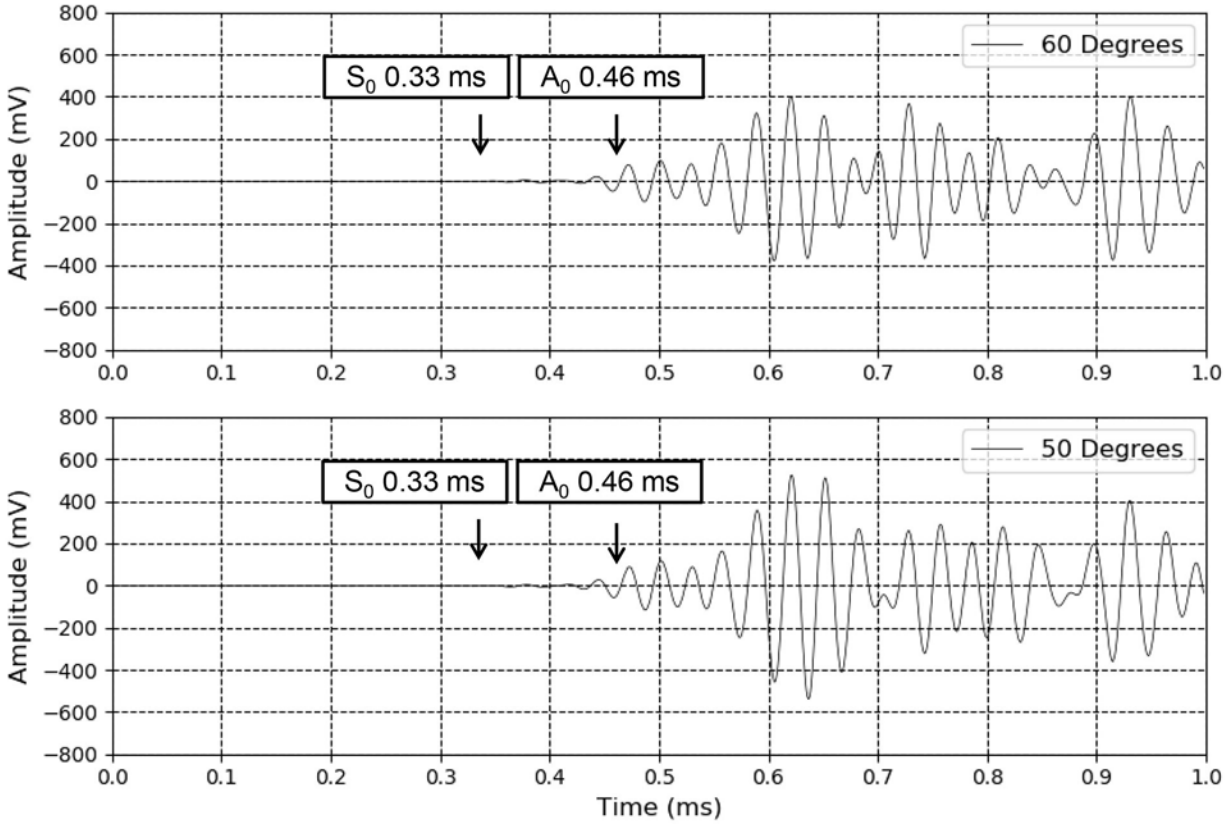

Figure B-2. A-scan of Laser Vibrometer Response with the Estimated Arrival Times of the S0 and A0 Signals Labeled for Transmitter Angle of 50° (*bottom*) and 60° (*top*)

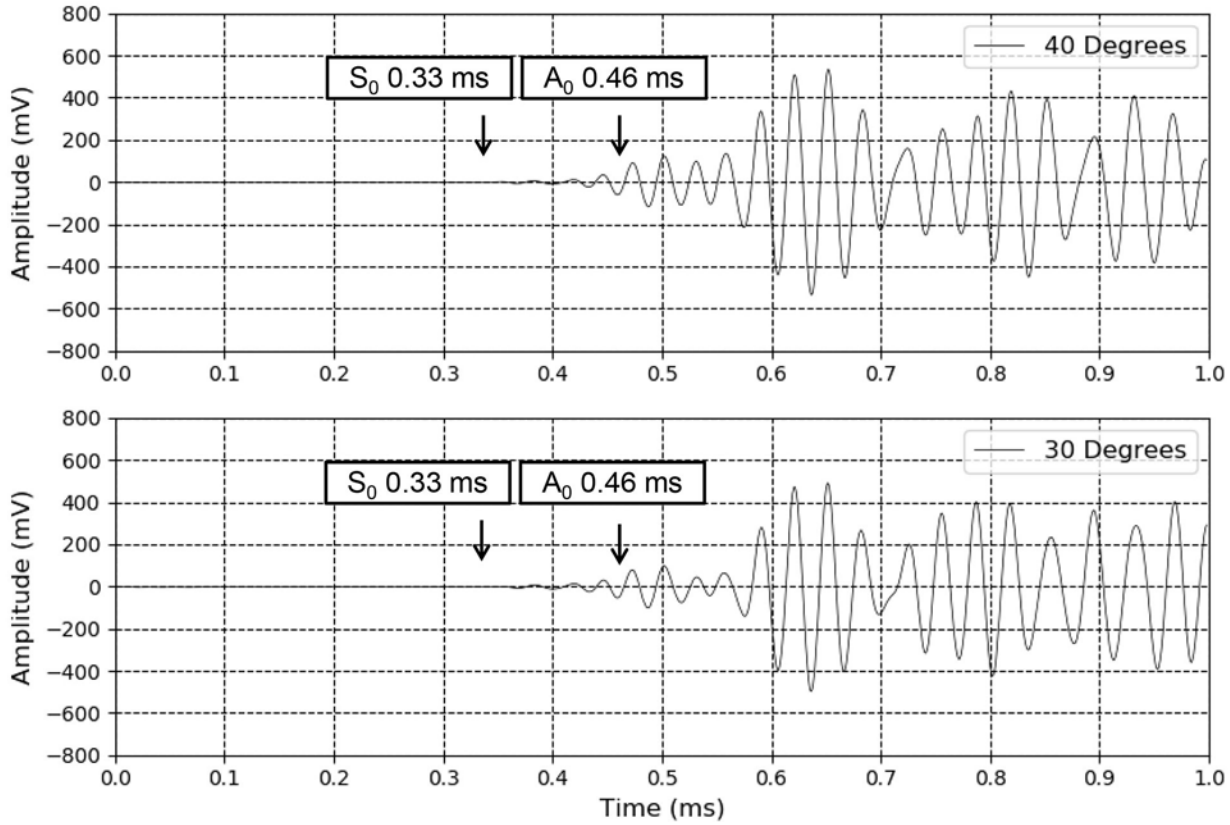

Figure B-3. A-scan of Laser Vibrometer Response with the Estimated Arrival Times of the S0 and A0 Signals Labeled for Transmitter Angle of 30° (*bottom*) and 40° (*top*)

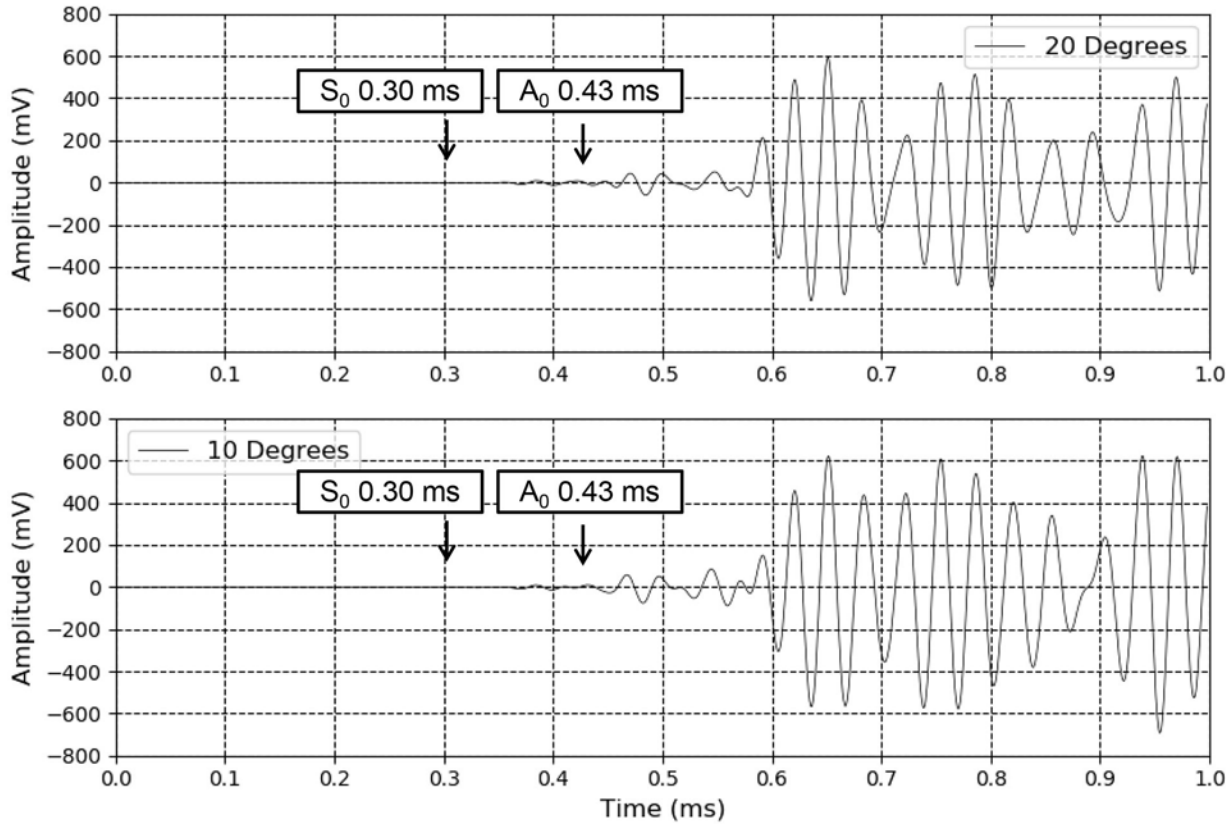

Figure B-4. A-scan of Laser Vibrometer Response with the Estimated Arrival Times of the S0 and A0 Signals Labeled for Transmitter Angle of 10° (*bottom*) and 20° (*top*)

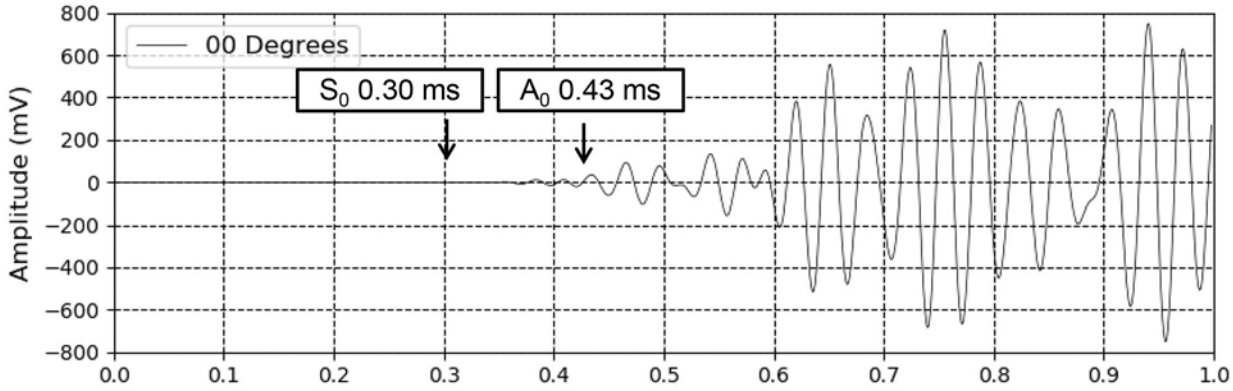

Figure B-5. A-scan of Laser Vibrometer Response with the Estimated Arrival Times of the S0 and A0 Signals Labeled for Transmitter Angle of 0°

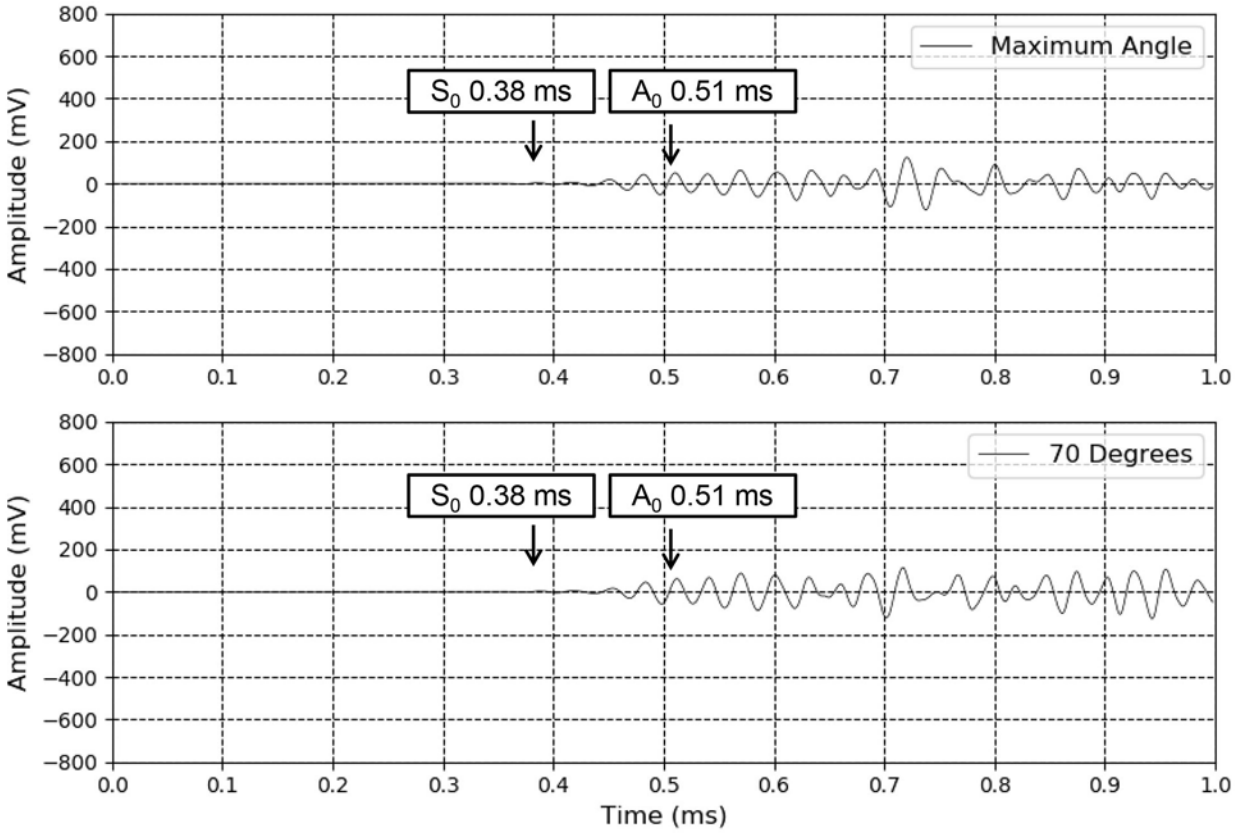

Figure B-6. A-scan of Piezoelectric Receiver Response with the Estimated Arrival Times of the S0 and A0 Signals Labeled for Transmitter Angle of 70° (*bottom*) and the Maximum Angle (*top*)

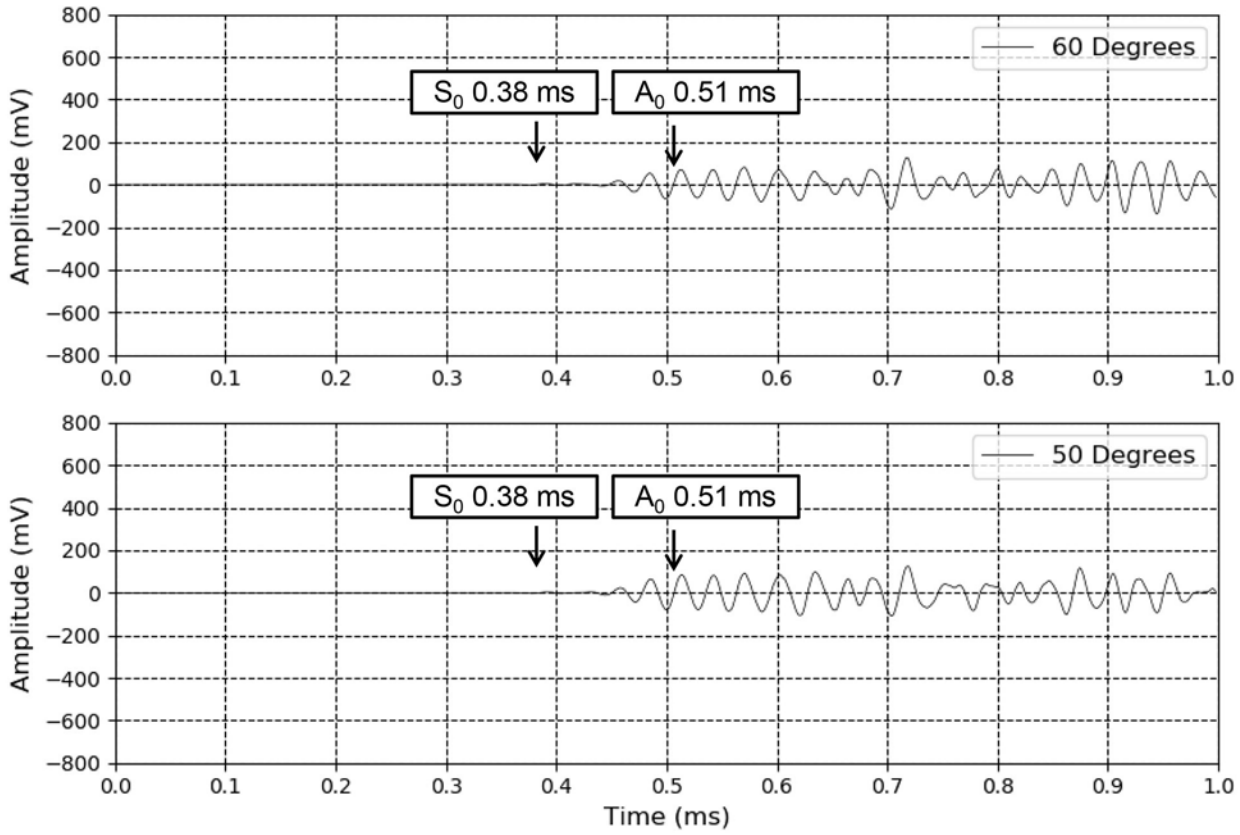

Figure B-7. A-scan of Piezoelectric Receiver Response with the Estimated Arrival Times of the S0 and A0 Signals Labeled for Transmitter Angle of 50° (*bottom*) and 60° (*top*)

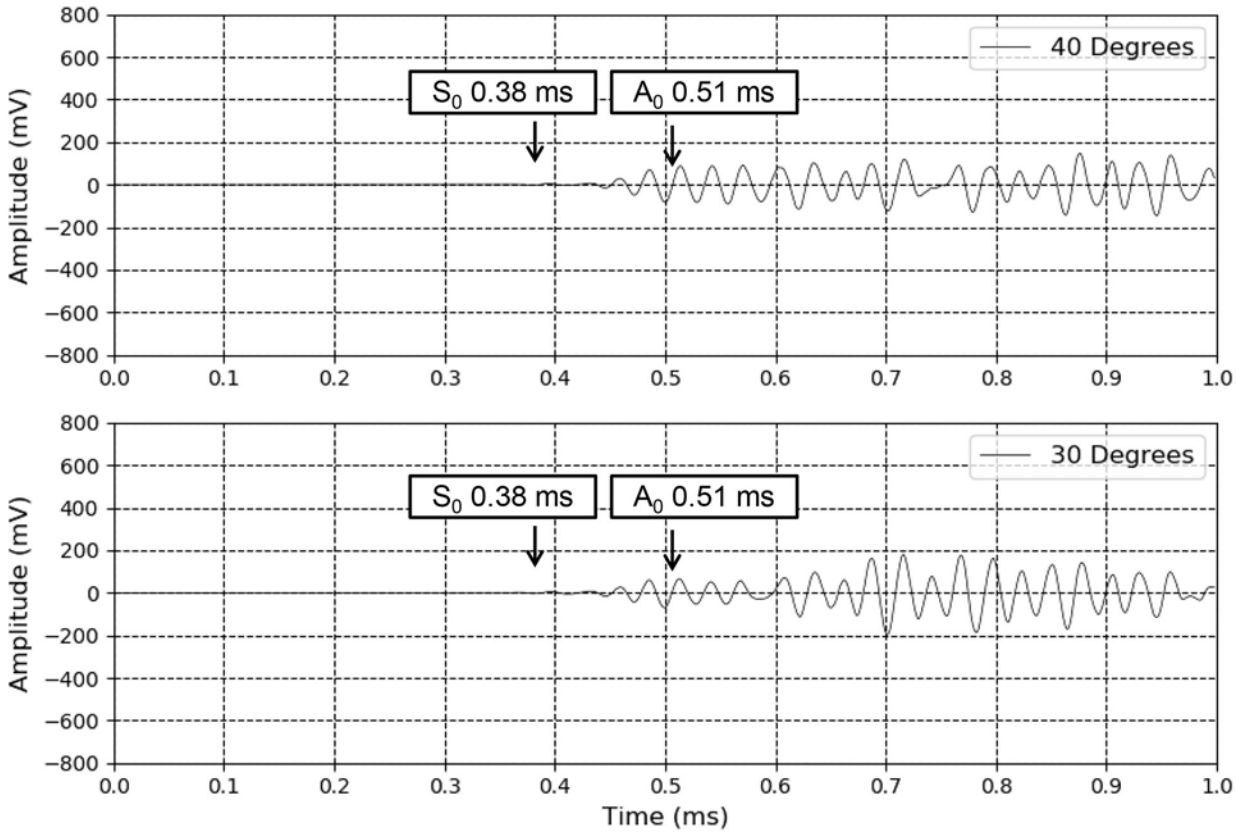

Figure B-8. A-scan of Piezoelectric Receiver Response with the Estimated Arrival Times of the S0 and A0 Signals Labeled for Transmitter Angle of 30° (*bottom*) and 40° (*top*)

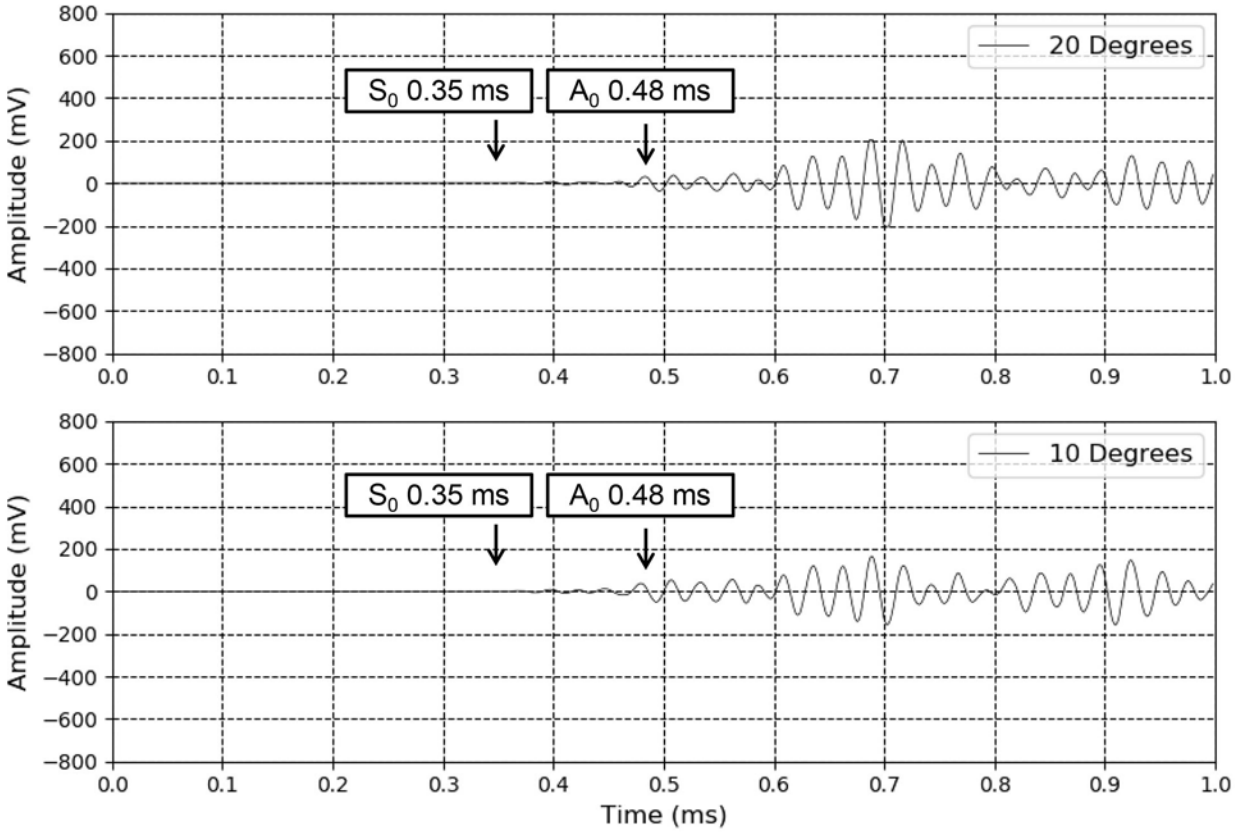

Figure B-9. A-scan of Piezoelectric Receiver Response with the Estimated Arrival Times of the S0 and A0 Signals Labeled for Transmitter Angle of 10° (*bottom*) and 20° (*top*)

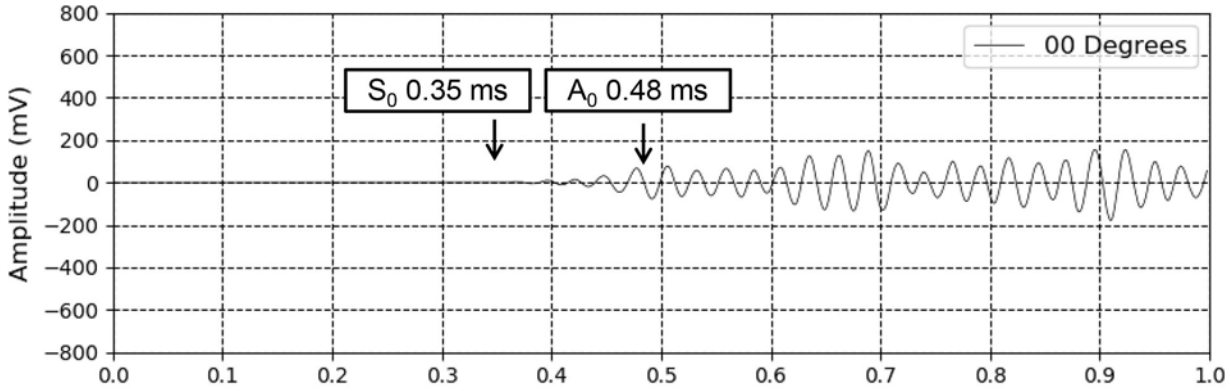

Figure B-10. A-scan of Piezoelectric Receiver Response with the Estimated Arrival Times of the S0 and A0 Signals Labeled for Transmitter Angle of 0°

This page is intentionally left blank.